

1 **Ensemble cloud-resolving modelling of a historic back-building mesoscale**  
2 **convective system over Liguria: The San Fruttuoso case of 1915**

3  
4 Antonio Parodi<sup>1</sup>, Luca Ferraris<sup>1,2</sup>, William Gallus<sup>3</sup>, Maurizio Maugeri<sup>4</sup>, Luca Molini<sup>1</sup>, Franco  
5 Siccardi<sup>1</sup>, and Giorgio Boni<sup>1,2</sup>

6  
7 1- CIMA Research Foundation, Savona, Italy

8 2- Dipartimento di Informatica, Bioingegneria, Robotica e Ingegneria dei Sistemi,  
9 University of Genoa, 16145 Genoa, Italy

10 3- Department of Geological and Atmospheric Sciences, Iowa State University, Ames, Iowa

11 4- Università degli Studi di Milano, Dipartimento di Fisica, Milan, Italy  
12

13 **Abstract**

14 Highly localized and persistent back-building mesoscale convective systems represent  
15 one of the most dangerous flash-flood producing storms in the north-western  
16 Mediterranean area. Substantial warming of the Mediterranean Sea in recent decades  
17 raises concerns over possible increases in frequency or intensity of these types of  
18 events as increased atmospheric temperatures generally support increases in water  
19 vapor content. However, analyses of the historical record do not provide a univocal  
20 answer, but these are likely affected by a lack of detailed observations for older  
21 events.

22 In the present study, 20<sup>th</sup> Century Reanalysis Project initial and boundary condition  
23 data in ensemble mode are used to address the feasibility of performing cloud-  
24 resolving simulations with 1 km horizontal grid spacing of a historic extreme event  
25 that occurred over Liguria: The San Fruttuoso case of 1915. The proposed approach  
26 focuses on the ensemble Weather Research and Forecasting (WRF) model runs that  
27 show strong convergence over the Liguria sea (17 out of 56 members), as these runs  
28 are the ones most likely to best simulate the event. It is found that these WRF runs  
29 generally do show wind and precipitation fields that are consistent with the occurrence  
30 of highly localized and persistent back-building mesoscale convective systems,  
31 although precipitation peak amounts are underestimated. Systematic small north-  
32 westward position errors with regard to the heaviest rain and strongest convergence  
33 areas imply that the Reanalysis members may not be adequately representing the  
34 amount of cool air over the Po Plain outflowing into the Liguria Sea through the  
35 Apennines gap. Regarding the role of historical data sources, this study shows that in  
36 addition to Reanalysis products, unconventional data, such as historical meteorological  
37 bulletins newspapers and even photographs can be very valuable sources of  
38 knowledge in the reconstruction of past extreme events.  
39

## 40 **1. Introduction**

41 Flash floods are phenomena very common to most Mediterranean coastal cities,  
42 accountable for millions of euros of damage and tens to hundreds of victims every  
43 year (Gaume et al. 2009). The north-western Mediterranean area is affected by such  
44 events in a period usually spanning from late summer (the end of August) to late fall  
45 (early December): in this period, the warm waters of the sea, in combination with  
46 large-scale meteorological systems coming from the Atlantic Ocean, provide a huge  
47 amount of energy, namely latent and sensible heat fluxes, to the atmosphere (Reale  
48 et al. 2001, Boni et al. 2006, Pinto et al. 2013). Heavy precipitation is then triggered  
49 by the typically very steep topography of the coasts: it is frequent to observe the  
50 monthly average rainfall to fall intensely in just a few hours and/or a significant  
51 fraction (up to 30-40%) of the yearly average in one day (Parodi et al 2012, Fiori et  
52 al. 2014). Obviously, the losses experienced in terms of human lives and economic  
53 damage in these very densely populated areas are often dramatic.

54 Among the flash flood producing storms in the Mediterranean area, a prominent  
55 feature is the highly localized and persistent back-building of mesoscale convective  
56 systems (MCSs, Schumacher and Johnson 2005, Duffourg et al. 2015, Violante et al.  
57 2016). Such a scenario has been observed often in the last decade, when Liguria (NW  
58 Italy) and Southern France have been repeatedly hit by severe floods: 2010 Varazze  
59 and Sestri Ponente, 2011 Cinqueterre and Genoa, 2012 Marseille and Isle du Levant,  
60 2014 Genoa and Chiavari, 2015 Nice. As shown in several recent works (Parodi et al.  
61 2012, Rebora et al. 2013, Fiori et al. 2014, Duffourg et al 2015, Silvestro et al. 2015,  
62 Cassola et al. 2016, Silvestro et al. 2016), convective cells, embedded in such MCSs,  
63 are generated on the sea by the convergence of a warm and moist south-easterly flow  
64 and a northerly much colder and drier one. These structures are then advected to the  
65 land where the combined action of the aforementioned currents and the topography  
66 force them to persist for several hours over a very localized area (e.g. about 100  
67 km<sup>2</sup>).

68 Many flood frequency studies have been carried out, focusing on rainfall regimes and  
69 Mediterranean flood seasonality and type (Barriendos et al. 2003, Llasat et al. 2005,  
70 Barriendos et al. 2006, Boni et al. 2006, Pinto et al. 2013, Llasat et al. 2014, Toreti et  
71 al. 2015). Due to the exploitation of both documentary sources and early  
72 measurements, these analyses have been able to go back several centuries, however,  
73 their results have been mostly inconclusive regarding changes in frequency of  
74 occurrence. Well-defined trends have not been found as usually flood frequency  
75 oscillates from period to period with no significant growth, not even in the most recent  
76 decades, regardless of the event's duration (a few hours to days).

77 The same result applies to precipitation extremes and their possible changes over the  
78 Mediterranean area in recent decades, studied by several authors, either by empirical  
79 or (mainly at-site) extreme value theory approaches (see e.g. Brunetti et al., 2001,  
80 2004, Alpert et al., 2002, Kostopoulou and Jones, 2005, Moberg et al., 2006, Brunet  
81 et al., 2007, Kioutsioukis et al., 2010, Rodrigo, 2010, Toreti et al., 2010, van den  
82 Besselaar et al., 2013). The temporal tendencies are not fully coherent throughout the  
83 region (Ulbrich et al., 2012) and rather conditioned by the specific site, the approach  
84 used and the period examined (Brugnara et al., 2012, Brunetti et al., 2012, Maugeri  
85 et al., 2015). On the contrary, an increase in precipitation extremes over the  
86 Mediterranean area is generally indicated by climate model scenarios (Alpert et al.,  
87 2002, Giorgi and Lionello, 2008, Trenberth, 2011).

88 It is therefore still an open debate whether the frequency of these phenomena is  
89 really increasing or if it is merely the perception of both the general public and  
90 scientific community. The latter hypothesis is supported by the fact that in the last  
91 10-20 years the observational capabilities have substantially increased. For example,  
92 in Italy alone, the remotely automated weather station network has grown to 5000  
93 stations offering an average density of about 1/75 station/km<sup>2</sup> with a 1 to 10-minute  
94 sampling rate. At the same time, the national weather radar network reached a fully  
95 operational coverage allowing for direct evaluation of the space-time structure of  
96 precipitation (Rebora et al. 2013).

97 Another factor contributing to enhance the perception of an increasing frequency of  
98 extreme precipitation and floods is that it has become much easier for weather-  
99 related disasters to make it to the news (Pasquaré and Oppizzi 2012, Grasso and  
100 Crisci 2016) and therefore to the general public. Moreover, a rapidly growing  
101 population and soil consumption increases the exposure of the population to such  
102 phenomena (Ward et al. 2013, European Environmental Agency, 2015).

103 To better investigate whether extreme precipitation and flood frequency are really  
104 increasing in the Mediterranean, it is important to improve the exploitation of the  
105 information available from past meteorological data. A contribution to this  
106 improvement may come from the development of methods that identify which  
107 ensemble analyses from projects like the 20th Century Reanalysis Project are able to  
108 produce precipitation fields that are reasonably intense and capable of causing  
109 extreme floods.

110 This paper focuses on a case study with the aim of investigating the ability of cloud-  
111 resolving grid spacing atmospheric simulations to capture the main features of an  
112 event causing a very severe flash flood. These simulations are performed using the  
113 Weather Research and Forecasting (WRF, Skamarock et al. 2005) numerical  
114 meteorological model forced by an ensemble of reanalysis fields from the 20<sup>th</sup> Century  
115 Reanalysis Project (Compo et al. 2006, Compo et al. 2011). The work is also  
116 important to reveal how well fine-scale models can simulate an event for which  
117 observations used to initialize the forcing model are extremely sparse (see section 4).  
118 One prior work, Michaelis and Lackmann (2013), showed some promising results in  
119 the use of WRF for another historical event, the New England Blizzard of 1888, but  
120 that event was a midlatitude cyclone driven by dynamics on a larger-scale. More on  
121 the windstorm modelling side, Stucki et al. (2015) reconstructed a 1925 high-impact  
122 foehn storm in the Swiss Alps.

123 In this study, the case under investigation was a very intense flash-flood producing  
124 event that occurred in 1915 in eastern Liguria (20-25 km east of Genoa, Liguria  
125 region capital city), affecting San Fruttuoso, a small hamlet near Portofino, and the  
126 coastal cities of Santa Margherita Ligure, Rapallo, and Chiavari (Figure 1). Based on  
127 the newspapers of the time and documentary sources, after relatively light rain during  
128 the night between September 24th and 25th, on the early morning of September 25<sup>th</sup>,  
129 the area was hit for a few hours (7-11 UTC) by violent rain that triggered widespread  
130 flash flooding, and a devastating debris flow. This landslide half-demolished the San  
131 Fruttuoso thousand-year old abbey and laid down a thick layer of sand and rocks to  
132 form a still existing 20-metre-wide 2-metre-deep beach (Faccini et al. 2008),  
133 nowadays a very popular seaside resort. Based both on the observations of the time  
134 (wind speed/direction, rainfall, observed lightnings) available for north-western Italy,  
135 and on the model simulations, the occurrence of a back-building MCS is suggested.

136 The paper is organized as follows. In Section 2 the 1915 convective event is  
137 presented. Section 3 describes the WRF model setting performed. Results are  
138 discussed in Section 4. Conclusions are drawn in Section 5.

139 **2. Meteorological scenario**

140 The synoptic and mesoscale information for this event are available both from the 20<sup>th</sup>  
141 Century Reanalysis Project (Compo et al. 2006, Compo et al. 2011) and from the  
142 weather bulletins issued on a daily basis by the Italian Royal Central Office for  
143 Meteorology (Regio Ufficio Centrale di Meteorologia e Geodinamica).

144 The 20<sup>th</sup> Century Reanalysis Project is an effort led by the Earth System Research  
145 Laboratory (ESRL) Physical Sciences Division (PSD) of the National Oceanic and  
146 Atmospheric Administration (NOAA) and the Cooperative Institute for Research in  
147 Environmental Sciences (CIRES) at the University of Colorado to produce a reanalysis  
148 dataset covering the entire twentieth century, assimilating only surface observations  
149 of synoptic pressure, monthly sea surface temperature and sea ice distribution. The  
150 observations have been assembled through international cooperation under the  
151 auspices of the Atmospheric Circulation Reconstructions over the Earth (ACRE)  
152 initiative, and working groups of Global Climate Observing System (GCOS) and World  
153 Climate Research Program (WCRP). The Project uses an Ensemble Filter data  
154 assimilation method, which directly yields each six-hourly analysis as the most likely  
155 state of the global atmosphere, and gives also estimates of the uncertainty in that  
156 analysis. This dataset provides the first estimates of global tropospheric variability  
157 spanning from 1851 to 2012 with a six-hourly temporal resolution and a 2.0° grid  
158 spacing. This study adopts 20<sup>th</sup> Century Reanalysis Project version 2C, which uses the  
159 same model as version 2 with new sea ice boundary conditions from the COBE-SST2  
160 (Hirahara et al. 2014), new pentad Simple Ocean Data Assimilation with sparse input  
161 (SODAsi.2) sea surface temperature fields (Giese et al. 2016), and additional  
162 observations from ISPD version 3.2.9 (Whitaker et al. 2004, Compo et al. 2013,  
163 Krueger et al. 2013, Hirahara et al. 2014, Cram et al. 2015).

164 The weather bulletins issued by the Italian Royal Central Office for Meteorology  
165 include weather maps at 7 UTC and 20 UTC and data (sea level pressure, wind  
166 (direction and speed), temperature, cloud cover, cloud direction, state of the sea,  
167 weather of the past 24 hours and notes) from about 125 Italian stations.

168 According to the reanalysis fields, the baroclinic circulation over Europe at 6 UTC of  
169 September 25<sup>th</sup>, (i.e. a few hours before the most intense phase of the event) is quite  
170 typical for heavy precipitation events over the study area, with an upper-level trough  
171 over Great Britain leading to a diffluent flow over the Liguria sea area, in combination  
172 with a widespread high pressure block on eastern Europe and southern Russia (Fig.  
173 2a). The diffluent flow over the Liguria sea area is associated with warm air advection  
174 at 850 hPa from the southern Mediterranean towards northern-western Mediterranean  
175 coastlines (Fig. 2b). Further information is provided by the mean sea level pressure  
176 (MSLP) field at the European scale: both the Italian weather map (7 UTC, Fig. 3a) and  
177 the reanalysis field (06 UTC, Figs. 2c and 3b) show an elongated trough over the  
178 western Mediterranean and a prominent ridge over south-eastern Europe,  
179 representing a blocking condition on the large-scale. The pressure gradient between  
180 the Gulf of Lyon and the Northern Adriatic Sea is about 12 hPa, according both to fig  
181 3a and 3b. The Italian weather map gives also evidence of a high pressure ridge  
182 extending into the Po Valley, which causes a significant surface pressure gradient  
183 between the western part of the Po Valley and the Liguria sea (about 3 hpa), as well  
184 as between the eastern and the western parts of the Po Valley (about 4 hPa). This  
185 high-pressure ridge is present in the reanalysis MSLP field too (06 UTC, Fig. 3b), even  
186 though it is much less evident than in the Italian weather map.

187 On the mesoscale, at 06 UTC, a significant 2-metre temperature difference, around 3-  
188 4 °C, is apparent from 20<sup>th</sup> Century Reanalysis Project fields between the Po Valley  
189 and the Liguria sea (Fig. 4a), as well as a significant 2-metre specific humidity



190 gradient (Fig. 4b). The temperature difference is also confirmed by the available  
191 observations at 07 UTC provided the Italian Royal Central Office for Meteorology (Fig.  
192 4c).

193 These mesoscale features represent the necessary ingredients for the generation of a  
194 back-building MCS offshore of the Liguria coastline, as observed in the 2010, 2011  
195 and 2014 high impact weather events in this region (Parodi et al. 2012, Reborra et al.  
196 2013, Fiori et al. 2014).

197 The back-building MCS hypothesis is supported by the 48-hour quantitative  
198 precipitation estimates (QPEs) for the period 24<sup>th</sup> September 07UTC - 26<sup>th</sup> September  
199 07UTC (Fig. 5). The raingauges (64) contributing to this map have been provided by  
200 different datasets such as the European Climate Assessment & Dataset project (Klein  
201 Tank et al. 2002, Klok and Klein Tank 2009), the KNMI Climate Explorer dataset  
202 (Trouet and Van Oldenborgh 2013), the Italian Meteorological Society (SMI, Auer et  
203 al. 2005), the Piedmont Region climatological dataset (Cortemiglia 1999), and the  
204 Chiavari Meteorological Observatory (Ansaloni 2006).

205 The QPE map shows clearly a v-shaped elongated pattern, very similar to the ones  
206 observed for the aforementioned events in Liguria. Based on historical information on  
207 sub-daily rain rates, it can be estimated that during the most intense phase of the  
208 event, the rainfall depths reached up to 400 mm in approximately 4 hours (7-11 UTC  
209 on September 25<sup>th</sup>) in some raingauges (Faccini et al. 2009): as a consequence of this  
210 intense and highly localized rainfall the coastal cities of Rapallo, Santa Margherita  
211 Ligure, Chiavari and San Fruttuoso suffered very serious damages (Fig. 6), with a  
212 death toll around 25-30 people. Interestingly, as in the case of the Genoa 2014 event,  
213 a very intense lightning activity was documented by the Italian Royal Central Office  
214 for Meteorology (Fig. 7).

215

### 216 **3. ARW-WRF model simulations**

217 The model simulations have been performed using the Advanced Research Weather  
218 Research and Forecasting Model (hereafter as ARW-WRF, version 3.4.1). Initial and  
219 boundary conditions were provided by the 20<sup>th</sup> Century Reanalysis Project Version  
220 version 2c (Compo et al. 2006, Compo et al. 2011) The ARW-WRF model was applied  
221 for each of the 56 members of the ensemble provided by the 20<sup>th</sup> Century Reanalysis  
222 Project database.

223 The ARW-WRF model is configured for this case study based on the results achieved in  
224 the ARF-WRF modelling of the Genoa 2011 and Genoa 2014 v-shape convective  
225 structures (Fiori et al. 2011, Fiori et al., 2017). Three nested domains (Fig. 8 panel a),  
226 centered on the Liguria region, were used with the outer nest d01 using 25 km  
227 horizontal grid spacing (61x55 grid points), the middle nest d02 using 5 km grid  
228 spacing (181x201 grid points) and the innermost nest d03 using 1 km grid spacing  
229 (526x526 grid points). Panels B-E (Fig. 8) provide the comparison between the  
230 topography over the D03 area, for D01, D02, D03, and the native 1 km grid spacing  
231 (for numerical stability reasons, given the very large number of ensemble members,  
232 initial conditions for domain D03-1 km are interpolated from D02-5 km, as in Fiori et  
233 al. 2014).

234 The benefits of a high number of vertical levels have been demonstrated in Fiori et al.  
235 (2014), and thus the same higher number of vertical levels (84) is adopted in this  
236 study. Since the grid-spacing ranges from the regional modelling limit (25 km) down  
237 to the cloud resolving one (1 km), two different strategies have been adopted with  
238 regard to convection parameterization. For the domain d01 we adopted the new

239 simplified Arakawa–Schubert scheme (Han and Pan 2011) as it is also used by the  
240 20<sup>th</sup> Century Reanalysis Project with 2.0° grid spacing. Conversely, a completely  
241 explicit treatment of convective processes has been carried out on the d02-5 km and  
242 d03-1 km domains (Fiori et al., 2014).

243 The double-Moment Thompson et al. (2008) scheme for microphysical processes has  
244 been adopted: this scheme takes into account ice species processes, whose relevance  
245 in this case study is confirmed by the intense lightning activity observed during the  
246 event, by modelling explicitly the spatio-temporal evolution of the intercept parameter  
247  $N_i$  for cloud ice. Furthermore, the Thompson scheme was shown to be the best  
248 performing for the Genoa 2011 and Genoa 2014 studies (Fiori et al. 2014 and 2017).  
249 With regard to the results in Fiori et al. (2014) about the role of the prescribed  
250 number of initial cloud droplets  $-N_{t_c}$ - created upon autoconversion of water vapour to  
251 cloud water and directly connected to peak rainfall amounts, a maritime value  
252 corresponding to a  $N_{t_c}$  of  $25 \cdot 10^6 \text{ m}^{-3}$  has been adopted.

253 It is important to highlight that the availability of the 56 members ensemble is a key  
254 strength in the present study, which enables estimates of uncertainties associated  
255 with dynamical downscaling down to the ARF-WRF d03-1 km domain.

256

#### 257 **4. Results and discussion**

258

259 A fundamental ingredient for the occurrence of back-building MCSs is the presence of  
260 a persistent and robust convergence line: the availability of a large 1 km ARF-WRF  
261 dynamically downscaled ensemble (56 members) allows the exploration of how many  
262 members produce such a convergence line over the northern part of the Liguria sea  
263 region where most of such MCSs form (Rebora et al. 2013). A convergence line is  
264 here classified as persistent and robust if the minimum value of the divergence within  
265 the study area is less than  $-7 \cdot 10^{-3} \text{ s}^{-1}$  for at least 4 hours in a row. The divergence  
266 threshold equal to  $-7 \cdot 10^{-3} \text{ s}^{-1}$  corresponds to the 99.95% percentile of the divergence  
267 values computed in every grid point within the region 7.50-10.25E / 43.75-44.50N in  
268 Fig. 8 for each ensemble member in the period 12UTC 24<sup>th</sup> September – 00UTC 26<sup>th</sup>  
269 September (with a 30-minute time resolution).

270 Using the above threshold, 17 of the 56 ARW-WRF runs (30% of the total) exhibit a  
271 persistent and robust convergence line in the considered period, while the remaining  
272 39 do not produce it or it is not persistent. In particular, the time series of divergence  
273 for four members (1, 13, 22, and 37 respectively) show that the minimum is reached  
274 (Fig. 9) at approximately the same time when hourly QPF (Quantitative Precipitation  
275 Forecast) exceeds 50 mm/h (Fig. 10, panels a-d, and g-l, members 1 and 13, Fig. 11,  
276 panels a-d, and g-l, members 22 and 37); the other 13 members are not shown as  
277 they behave very similarly. The four representative members exhibit also large QPFs  
278 over the whole 36 hours of the simulations (Fig. 10, panels f and n, members 1 and  
279 13, Fig. 11, panels f and n, members 22 and 37), even though significant differences  
280 both in the total amount and in the spatial distribution are found. Significant values of  
281 the Lightning Potential Index (LPI, Yair et al. 2010), in good agreement with the  
282 observations of the Italian Royal Central Office for Meteorology, are shown in Fig. 10  
283 (panels e and m, members 1 and 13) and Fig. 11, (panels e and m, members 22 and  
284 37).

285 Yet, most of the back-building MCS-producing members are affected by a non-  
286 negligible location error (see panels f and n of Figures 10 and 11 for the four selected  
287 members) with respect to the observed daily rainfall map (Fig. 5). This feature is  
288 largely due to a predominance of the south-easterly wind component over the north-

289 westerly one (coming from Po Valley), thus pushing the convergence line too north-  
290 westwards (red dashed line), close to the western Liguria coastline. This discrepancy  
291 is explained by the highly localized spatio-temporal nature of this event, by the  
292 comparatively low spatial density of the surface pressure stations assimilated by the  
293 20<sup>th</sup> Century Reanalysis Project over the western Mediterranean region (Fig. 12) and  
294 by the relatively coarse characteristics (2.0° grid spacing, and 6-hourly temporal  
295 resolution) of the 20<sup>th</sup> Century Reanalysis Project forcing initial and boundary  
296 conditions data. For instance, the primary wind convergence area over the sea and  
297 the inland area affected by the rainfall (6.5-10.5° E / 43.5-45.5° N) is represented by  
298 only a few (2-3) 20<sup>th</sup> Century Reanalysis Project grid points.

299 To quantitatively examine precipitation errors for each ARW-WRF ensemble member,  
300 a bias and mean absolute error (MAE) analysis of the 36 hour (12UTC 24/09 – 00UTC  
301 26/09) QPF versus the 48 hour QPE (07UTC 24/09 – 07UTC 26/09) is undertaken by  
302 comparing the available 64 raingauges with the nearest grid points of the d03-1 km.  
303 The use of different time periods for QPE and QPF is not an issue as most of the  
304 observed precipitation reported for Liguria fell in a time span encompassed in the run  
305 time of the simulations. The results (Fig. 13) show that most of the 56 ARF-WRF  
306 members have a negative BIAS of roughly 10-40 mm, largely explained by the  
307 ensemble widespread underestimation of the extreme rainfall depths over the coastal  
308 cities of Santa Margherita Ligure, Rapallo, and Chiavari. The 17 selected members  
309 (red markers) show an average BIAS of -22 mm and a MAE of 40 mm, while the  
310 remaining 39 members have an average BIAS of -31 mm and a MAE of 42 mm. Also  
311 for the 17 selected members, the BIAS is largely explained by the stations mostly  
312 affected by the MCS and it reduces to -8 mm when Chiavari, Cervara and S.  
313 Margherita Ligure are excluded from the comparison.

314 Because traditional verification measures (e.g. point-to-point verification measures)  
315 applied to QPF are greatly influenced by location errors (Mass et al. 2002), a deeper  
316 understanding of QPF performance in the WRF ensemble is gained by performing  
317 object based verification using the Method for Object-based Diagnostic Evaluation  
318 (MODE, Davis et al. 2006a, 2006b), intended to reproduce a human analyst's  
319 evaluation of the forecast performance. The MODE analysis is performed using a  
320 multi-step automated process. A convolution filter is applied to the raw field to  
321 identify the objects. When the objects are identified, some attributes regarding  
322 geometrical features of the objects (such as location, size, aspect ratio and  
323 complexity) and precipitation intensity (percentiles, etc.) are computed. These  
324 attributes are used to merge objects within the same forecast/observation field, to  
325 match forecast and observed objects and to summarize the performance of the  
326 forecast by attribute comparison. Finally, the interest value combines in a total  
327 interest function the attributes (the centroid distance, the boundary distance, the  
328 convex hull distance, the orientation angle difference, the object area ratio, the  
329 intersection divided by the union area ratio, the complexity ratio, and the intensity  
330 ratio) computed in the object analysis, providing an indicator of the overall  
331 performance of matching and merging between observed and simulated objects. In  
332 the present study, the relative weight of each attribute used the default setting in  
333 MODE (National Center for Atmospheric Research (NCAR), 2013). The displacement  
334 errors including centroid distance and boundary distance were weighted the greatest  
335 in the calculation of total interest.

336 In our experiment we have empirically chosen the convolution disk radius and  
337 convolution threshold, so that this choice would recognize precipitation areas (at least  
338 roughly 50x50 km or so) similar to what a human would identify. For each ARF-WRF  
339 ensemble member the 36-hour (12UTC 24/09 – 00UTC 26/09) QPF is compared with  
340 the 48-hour QPE (07UTC 24/09 – 07UTC 26/09), both bilinearly interpolated to the

341 same 10 km grid. This grid spacing represents a good compromise between the native  
342 1 km ARF-WRF grid spacing and the 40 km average distance between the available 64  
343 raingauges. After a set of experiments, we fixed the value of the convolution radius to  
344 one grid point and the threshold of the convoluted field to 75 mm. Twelve members  
345 out of the 17 members selected using the minimum divergence criterion show  
346 significant values (above 0.8) of the total interest function (Tab. 1). This value is  
347 slightly higher than the default one (0.7) used by MODE to match paired objects, in  
348 order to restrict our analysis to the best simulated events. Despite the limited  
349 observations available in 1915, our ensemble performs relatively well when  
350 considering object-based parameters. Specifically, when examining paired observed  
351 and modelled clusters, these twelve members demonstrate useful skill for: centroid  
352 distance, providing a quantitative sense of spatial displacement of forecast; forecast  
353 area/observed area, providing an objective measure of over-or under-prediction of  
354 areal extent of the forecasts; forecast intensity 50/observed intensity 50 and forecast  
355 intensity 90/observed intensity 90, providing objective measures of median (50th  
356 percentile) and near-peak (90th percentile) intensities found in the objects; and the  
357 already mentioned total interest, a summary statistic derived from the fuzzy logic  
358 engine with user-defined interest maps for all these attributes plus some others (Tab.  
359 1).

360 Indeed it is impressive that small displacement errors averaging only 114 km with a  
361 standard displacement of only 62 km are obtained despite the very crude initialization  
362 of a 1915 reanalysis case. In a much more recent set of cases, Duda and Gallus  
363 (2013) found an average displacement distance (absolute error) of 105 km for  
364 initiation of systems. Squitieri and Gallus (2016) show that centroids of forecasted  
365 MCSs in their sample of 31 relatively recent events in the United States Central Plains  
366 are usually over 100 km or more removed from the centroids of the observed MCSs.  
367 Similarly good performance of the ensemble exists for areal coverage, rainfall  
368 intensity (although there is a 30-40% underestimate), and overall characteristics of  
369 the forecasted objects as implied by the interest value.

370 Selected members 1, 13, 22 and 37 (Fig. 14) have total interest values above 0.93  
371 (close to 1 is good) and their paired clusters distance, namely the distance between  
372 centroids of observed and simulated rain regions, is around 100 km.

373 The availability of high resolution simulations allows one to gain a deeper  
374 understanding of the dynamics of the San Fruttuoso 1915 storm evolution. The  
375 physical mechanism responsible for the generation of the back-building mesoscale  
376 convective systems in this area has been recently explained by Fiori et al. (2017).  
377 Taking advantage of the availability of both observational data and modelling results  
378 at the micro- $\alpha$  meteorological scale, Fiori et al. (2017) provide insights about the  
379 triggering mechanism and the subsequent spatio-temporal evolution of the Genoa  
380 2014 back-building MCS. The major finding is the important effect of a virtual  
381 mountain created on the Ligurian sea by the convergence of a cold and dry jet  
382 outflowing from the Po valley and a warm and moist low level south-easterly jet  
383 within the planetary boundary layer.

384 The same mechanism is active also for this case. Let us consider, as an example the  
385 convective flow field at 06UTC on 25 September 1915 (see Fig. 15), as predicted by  
386 member 1 of the ensemble. Panel A shows the 2 m potential temperature field  
387 together with the 10 m horizontal wind vector field: the colder and drier jet outflowing  
388 from the Po valley and the warmer and moister air from the southern Mediterranean  
389 Sea are evident. Panel A shows, by means of the green dotted cross section (45°),  
390 also the thin potential temperature layer (virtual mountain) in front of the actual  
391 Liguria topography (panel b). This acts, as described in Fiori et al. (2017), to produce  
392 strong convective cells in panel c (updraft velocity above 10 m/s) with the apparent

393 back-building on the western side (less mature and intense cells around 8.4°  
394 latitude). The main updraft produces vertical advection of water vapor (panel d), thus  
395 resulting in significant production of rainwater (panel e), snow (panel f, significantly  
396 advected inland by the upper level south-westerly winds), and graupel (panel g).

## 397 **5. Conclusions**

398 Highly localized and persistent back-building MCSs represent one of the most  
399 dangerous flash-flood producing storms in the north-western Mediterranean area. A  
400 historic extreme precipitation event occurring over Liguria on September 1915, which  
401 seems to be due to one of these systems, was investigated in this paper both by  
402 means of a large collection of observational data and by means of atmospheric  
403 simulations performed using the ARF-WRF model forced by an ensemble of reanalysis  
404 fields from the 20<sup>th</sup> Century Reanalysis Project.

405 The results show that the simulated circulation features are consistent with the  
406 hypothesis of a highly localized back-building MCS over Liguria sea, and that the ARF-  
407 WRF runs -driven by a significant fraction of the members of the 20<sup>th</sup> Century  
408 Reanalysis Project ensemble- produce fields that are in reasonable agreement with  
409 the observed data.

410 The proposed approach was to focus only on the ARF-WRF runs showing strong  
411 convergence so as to get the best depiction of the event. Thus, we suggest that, when  
412 using datasets such as the 20<sup>th</sup> Century Reanalysis Project, it is important to consider  
413 that the physics/dynamics are likely to play a role in the events of interest, and to  
414 follow a similar technique to selectively use the Reanalysis ensemble members best  
415 displaying the key physics/dynamics of the event. Future work should test further an  
416 approach like this one to get a better understanding of how well the same  
417 convergence detection approach in regional climate model simulations of past and  
418 future climate (e.g. Pieri et al. 2015 at cloud-permitting grid spacing) can quantify  
419 possible changes in back-building MCS precipitation processes.

420 On the data collection side, this study showed that in addition to the use of Reanalysis  
421 products, other sources of data, such as newspapers, photographs, and historical  
422 meteorological bulletins can be essential sources of knowledge. Focusing on historical  
423 meteorological bulletins, future work on this particular case and similar ones occurring  
424 along the north-western Mediterranean coastline will explore the use of bogus  
425 observations or other preprocessing techniques to alter lower tropospheric conditions  
426 at model initialization time to better match actual observations, which may result in a  
427 better location of the convergence line and consequently simulation of the  
428 precipitation event.

429

## 430 **6. Acknowledgments**

431 This work was supported by the Italian Civil Protection Department and by the  
432 Regione Liguria. The ground based observations were provided by Italian Civil  
433 Protection Department and the Ligurian Environmental Agency. The raingauge data  
434 were courtesy of the European Climate Assessment & Dataset project, the KNMI  
435 Climate Explorer dataset, the Italian Meteorological Society, Piedmont Region  
436 climatological dataset, and the Chiavari Meteorological Observatory. Antonio Parodi  
437 would like also to acknowledge the support of the FP7 DRIHM (Distributed Research  
438 Infrastructure for Hydro-Meteorology, 2011-2015) project (contract number 283568).  
439 Thanks are due to the CINECA, where the numerical simulations were performed on  
440 the Galileo System, Project-ID: SCENE. W. Gallus appreciates the opportunity for a  
441 research visit at the University of Milan.

442 **7. References**

- 443 Alpert, P., Ben-Gai, T., Baharad, A., Benjamini, Y., Yekutieli, D., Colacino, M.,  
444 Diodato, L., Ramis, C., Homar, V., Romero, R., Michaelides, S., & Manes, A. (2002).  
445 The paradoxical increase of Mediterranean extreme daily rainfall in spite of decrease  
446 in total values. *Geophys. Res. Lett.*, 29(11).  
447
- 448 Ansaloni, A. (2006). The Observatory at Chiavari, Italy: its history and museum.  
449 *Weather*, 61(10), 283-285.  
450
- 451 Auer, I., Boehm, R., Jurkovic, A., Orlik, A., Potzmann, R., Schoener, W., Ungersboeck,  
452 M., Brunetti, M., Nanni, T., Maugeri, M., Briffa, K., Jones, P., Efthymiadis, D., Mestre,  
453 O., Moisseline, J.M., Begert, M., Brazdil, R., Bochnicek, O., Cegnar, T., Garjic-Capka,  
454 M., Zaninovic, K., Majstorovic, Z., Szalai, S., Szentimery, T., & Mercalli, L. (2005). A  
455 new instrumental Precipitation Dataset for the Greater Alpine Region for the period  
456 1800-2002. *Int. J. Climatol.*, 25(2), 139-166.  
457
- 458 Barriendos, M., Coeur, D., Lang, M., Llasat, M. C., Naulet, R., Lemaître, D., & Barrera,  
459 A. (2003). Stationarity analysis of historical flood series in France and Spain (14th–  
460 20th centuries). *Natural Hazards and Earth System Science*, 3(6), 583-592.  
461
- 462 Barriendos, M., & Rodrigo, F. S. (2006). Study of historical flood events on Spanish  
463 rivers using documentary data. *Hydrological Sciences Journal*, 51(5), 765-783.  
464
- 465 Boni, G., Parodi, A., & Rudari, R. (2006). Extreme rainfall events: Learning from  
466 raingauge time series. *Journal of hydrology*, 327(3), 304-314.  
467
- 468 Brugnara, Y., Brunetti, M., Maugeri, M., Nanni, T., & Simolo, C. (2012). High-  
469 resolution analysis of daily precipitation trends in the central Alps over the last  
470 century. *International Journal of Climatology*, 32(9), 1406-1422.  
471
- 472 Brunet, M., Jones, P. D., Sigró, J., Saladié, O., Aguilar, E., Moberg, A., Della-Marta,  
473 P.M., Lister, D., Walther, A., & López, D. (2007). Temporal and spatial temperature  
474 variability and change over Spain during 1850–2005. *Journal of Geophysical*  
475 *Research: Atmospheres*, 112(D12).  
476
- 477 Brunetti, M., Maugeri, M., & Nanni, T. (2001). Changes in total precipitation, rainy  
478 days and extreme events in northeastern Italy. *International Journal of Climatology*,  
479 21(7), 861-871.  
480
- 481 Brunetti, M., Buffoni, L., Mangianti, F., Maugeri, M., & Nanni, T. (2004). Temperature,  
482 precipitation and extreme events during the last century in Italy. *Global and planetary*  
483 *change*, 40(1), 141-149.  
484
- 485 Brunetti, M., Caloiero, T., Coscarelli, R., Gullà, G., Nanni, T., & Simolo, C. (2012).  
486 Precipitation variability and change in the Calabria region (Italy) from a high  
487 resolution daily dataset. *International Journal of Climatology*, 32(1), 57-73.  
488
- 489 Cassola, F., Ferrari, F., Mazzino, A., & Miglietta, M. M. (2016). The role of the sea on  
490 the flash floods events over Liguria (northwestern Italy). *Geophysical Research*  
491 *Letters*, 43(7), 3534-3542.  
492

493 Compo, G. P., Whitaker, J. S., & Sardeshmukh, P. D. (2006). Feasibility of a 100-year  
494 reanalysis using only surface pressure data. *Bulletin of the American Meteorological*  
495 *Society*, 87(2), 175-190.

496

497 Compo, G.P., Whitaker, J.S., Sardeshmukh, P.D., Matsui, N., Allan, R.J., Yin, X.,  
498 Gleason Jr, B.E, Vose, R.S., Rutledge, G., Bessemoulin, P., Brönnimann, S., Brunet,  
499 M., Crouthamel, R.I., Grant, A.N., Groisman, P.Y., Jones, P.D., Kruk, M., Kruger, A.C.,  
500 Marshall, G.J., Maugeri, M., Mok, H.Y., Nordli, Ø., Ross, T.F., Trigo, R.M., Wang, X.L.,  
501 Woodruff, S.D., & Worley, S.J., (2011). The twentieth century reanalysis project.  
502 *Quarterly Journal of the Royal Meteorological Society*, 137(654), 1-28.

503

504 Compo, G. P., Sardeshmukh, P. D., Whitaker, J. S., Brohan, P., Jones, P. D., & McColl,  
505 C. (2013). Independent confirmation of global land warming without the use of station  
506 temperatures. *Geophysical Research Letters*, 40(12), 3170-3174.

507

508 Cortemiglia, G. C. (1999). Serie climatiche ultracentenarie (con allegato CD ROM).  
509 Collana Studi Climatologici in Piemonte, Regione Piemonte, 3, 1-92.

510

511 Cram, T.A., Compo, G.P., Yin, X., Allan, R.J., McColl, C., Vose, R.S., Whitaker, J.S.,  
512 Matsui, N., Ashcroft, I., Auchmann, R., Bessemoulin, P., Brandsma, T., Brohan, P.,  
513 Brunet, M., Comeaux, J., Crouthamel, R., Gleason B.E. Jr, Groisman, P.Y., Hersbach,  
514 H., Jones, P.D., Jónsson, T., Jourdain, S., Kelly, G., Knapp, K.R., Kruger, A., Kubota,  
515 H., Lentini, G., Lorrey, A., Lott, N., Lubker, S.J., Luterbacher, J., Marshall, G.J.,  
516 Maugeri, M., Mock, C.J., Mok, H.J., Nordli, O., Rodwell, M.J., Ross, T.F., Schuster, D.,  
517 Srncac, L., Valente, M.A., Vizi, Z., Wang, X.L., Westcott, N., Woollen, J.S., & Worley,  
518 S.J. (2015). The international surface pressure databank version 2. *Geoscience Data*  
519 *Journal*, 2(1), 31-46.

520

521 Davis, C., B. Brown, & R. Bullock, 2006a: Object-based verification of precipitation  
522 forecasts. Part I: Methods and application to mesoscale rain areas. *Mon. Wea. Rev.*,  
523 134, 1772–1784.

524

525 Davis, C., B. Brown, & R. Bullock, 2006b: Object-based verification of precipitation  
526 forecasts. Part II: Application to convective rain systems. *Mon. Wea. Rev.*, 134, 1785–  
527 1795.

528

529 Duda, J. D., & Gallus Jr, W. A., 2013: The Impact of Large-Scale Forcing on Skill of  
530 Simulated Convective Initiation and Upscale Evolution with Convection-Allowing Grid  
531 Spacings in the WRF\*. *Weather and Forecasting*, 28(4), 994-1018.

532

533 Duffourg, F., Nuissier, O., Ducrocq, V., Flamant, C., Chazette, P., Delanoe, J.,  
534 Doerenbecher, A., Fourrié, N., Di Girolamo, P., Lac, C., Legain, D., Martinet, M., Said,  
535 F., & Bock, O. ... & Legain, D. (2015). Offshore deep convection initiation and  
536 maintenance during IOP16a Offshore deep convection initiation and maintenance  
537 during HyMeX IOP 16a heavy precipitation event. *Quarterly Journal of the Royal*  
538 *Meteorological Society*. 142: 259–274.

539

540 European Environmental Agency (2015), SOER 2015 — The European environment —  
541 state and outlook 2015 A comprehensive assessment of the European environment's  
542 state, trends and prospects, in a global context.

543

544 Faccini, F., Piccazzo, M., & Robbiano, A. (2009). Natural hazards in San Fruttuoso of  
545 Camogli (Portofino Park, Italy): a case study of a debris flow in a coastal environment.  
546 *Bollettino della Societa Geologica Italiana*, 128(3), 641-654.  
547

548 Fiori, E., Comellas, A., Molini, L., Rebora, N., Siccardi, F., Gochis, D. J., Tanelli, S., &  
549 Parodi, A. (2014). Analysis and hindcast simulations of an extreme rainfall event in  
550 the Mediterranean area: The Genoa 2011 case. *Atmospheric Research*, 138, 13-29.  
551

552 Fiori, E., Ferraris, L., Molini, L., Siccardi, F., Kranzlmüller, D. & Parodi, A. (2017),  
553 Triggering and evolution of a deep convective system in the Mediterranean Sea:  
554 modelling and observations at a very fine scale. *Q.J.R. Meteorol. Soc.*  
555 doi:10.1002/qj.2977.  
556

557 Gaume, E., Bain, V., Bernardara, P., Newinger, O., Barbuc, M., Bateman, A.,  
558 Blaškovicová, L., Blöschl, G., Borga, M., Dumitrescu, A., Daliakopoulos, J., Garcia, J.,  
559 Irimescu, A., Kohnova, S., Koutroulis, A., Marchi, L., Matreata, S., Medina, V., Preciso,  
560 E., Sempere-Torres, D., Stancalie, G., Szolgay, J., Tsanis, J., Velascom, D., &  
561 Viglione, A. (2009). A compilation of data on European flash floods. *Journal of*  
562 *Hydrology*, 367(1), 70-78.  
563

564 Giese, B. S., Seidel, H. F., Compo, G. P., & Sardeshmukh, P. D. (2016). An ensemble  
565 of ocean reanalyses for 1815–2013 with sparse observational input. *Journal of*  
566 *Geophysical Research: Oceans*.  
567

568 Giorgi, F., & Lionello, P. (2008). Climate change projections for the Mediterranean  
569 region. *Global and Planetary Change*, 63(2), 90-104.  
570

571 Grasso, V., & Crisci, A. (2016). Codified hashtags for weather warning on Twitter: an  
572 Italian case study. *PLoS currents*, 8.  
573

574 Han, J., & Pan, H. L. (2011). Revision of convection and vertical diffusion schemes in  
575 the NCEP global forecast system. *Weather and Forecasting*, 26(4), 520-533.  
576

577 Hirahara, S., Ishii, M., & Fukuda, Y. (2014). Centennial-scale sea surface temperature  
578 analysis and its uncertainty. *Journal of Climate*, 27(1), 57-75.  
579

580 Klein Tank, A.M.G., Wijngaard, J.B., Können, G.P., Böhm, R., Demarée, G., Gocheva,  
581 A., Mileta M., Pashiardis, S., Hejkrlik, L., Kern-Hansen, C., Heino, R., Bessemoulin, P.,  
582 Müller-Westmeier, G., Tzanakou, M., Szalai, S., Pálsdóttir, T., Fitzgerald, D., Rubin,  
583 S., Capaldo, M., Maugeri, M., Leitass, A., Bukantis, A., Aberfeld, R., van Engelen,  
584 A.F.V., Forland, E., Miletus, M., Coelho, F., Mares, C., Razuvaev, V., Nieplova, E.,  
585 Cegnar, T., Antonio López, J., Dahlström, B., Moberg, A., Kirchhofer, W., Ceylan, A.,  
586 Pachaliuk, O., Alexander, L.V., & Petrovic, P. (2002). Daily dataset of 20th - century  
587 surface air temperature and precipitation series for the European Climate Assessment.  
588 *International journal of climatology*, 22(12), 1441-1453.  
589

590 Klok, E. J., & Klein Tank, A. M. G. (2009). Updated and extended European dataset of  
591 daily climate observations. *International Journal of Climatology*, 29(8), 1182-1191.  
592

593 Kioutsioukis, I., Melas, D., & Zerefos, C. (2010). Statistical assessment of changes in  
594 climate extremes over Greece (1955–2002). *International Journal of Climatology*,  
595 30(11), 1723-1737.  
596



597 Kostopoulou, E., & Jones, P. D. (2005). Assessment of climate extremes in the  
598 Eastern Mediterranean. *Meteorology and Atmospheric Physics*, 89(1-4), 69-85.  
599

600 Krueger, O., Schenk, F., Feser, F., & Weisse, R. (2013). Inconsistencies between long-  
601 term trends in storminess derived from the 20CR reanalysis and observations. *Journal*  
602 *of Climate*, 26(3), 868-874.  
603

604 Llasat, M. C., Barriendos, M., Barrera, A., & Rigo, T. (2005). Floods in Catalonia (NE  
605 Spain) since the 14th century. Climatological and meteorological aspects from  
606 historical documentary sources and old instrumental records. *Journal of Hydrology*,  
607 313(1), 32-47.  
608

609 Llasat, M. C., Marcos, R., Llasat-Botija, M., Gilabert, J., Turco, M., & Quintana-Seguí,  
610 P. (2014). Flash flood evolution in North-Western Mediterranean. *Atmospheric*  
611 *Research*, 149, 230-243.  
612

613 Maugeri, M., Brunetti, M., Garzoglio, M., & Simolo, C. (2015). High-resolution analysis  
614 of 1 day extreme precipitation in Sicily. *Natural Hazards and Earth System Science*,  
615 15(10), 2347-2358.  
616

617 Mass, C. F., Ovens, D., Westrick, K., & Colle, B. A. (2002). Does increasing horizontal  
618 resolution produce more skillful forecasts?. *Bulletin of the American Meteorological*  
619 *Society*, 83(3), 407-430.  
620

621 Michaelis, A. C., & Lackmann, G. M. (2013), Numerical modelling of a historic storm:  
622 Simulating the Blizzard of 1888. *Geophysical Res. Letters*, 40, 4092-4097.  
623

624 Moberg, A., Jones, P.D., Lister, D., Alexander, W., Brunet, M., Jacobeit, J., Alexander,  
625 L.V., Della-Marta, P.M., Luterbacher, J., Yiou, P., Chen, D., Klein Tank, A.M.G.,  
626 Saladié, O., Sigró, J., Aguilar, E., Alexandersson, H., Almarza, C., Auer, I., Barriendos,  
627 M., Begert, M., Bergström, H., Böhm, R., Butler, C.J., Caesar, J., Drebs, A., Founda,  
628 D., Gerstengarbe, F.W., Micela, G., Maugeri, M., Österle, H., Pandzic, K., Petrakis, M.,  
629 Srnec, L., Tolasz, R., Tuomenvirta, H., Werner, P.C., Linderholm, H., Philipp, A.,  
630 Wanner, H., & Xoplaki, E. (2006). Indices for daily temperature and precipitation  
631 extremes in Europe analyzed for the period 1901–2000. *Journal of Geophysical*  
632 *Research: Atmospheres*, 111, D22106.  
633

634 National Center for Atmospheric Research (NCAR) (2013). Model Evaluation Tools  
635 version 4.1 (METv4.1): User's guide 4.1. Developmental Testbed Center Rep., 226 pp.  
636 [Available online at  
637 [http://www.dtcenter.org/met/users/docs/users\\_guide/MET\\_Users\\_Guide\\_v4.1.pdf](http://www.dtcenter.org/met/users/docs/users_guide/MET_Users_Guide_v4.1.pdf).]  
638

639 Parodi, A., Boni, G., Ferraris, L., Siccardi, F., Pagliara, P., Trovatore, E., Fofoula-  
640 Georgiou, E., & Kranzlmüller, D. (2012). The "perfect storm": From across the  
641 Atlantic to the hills of Genoa. *Eos, Transactions American Geophysical Union*, 93(24),  
642 225-226.  
643

644 Pasquaré, F. A., & Oppizzi, P. (2012). How do the media affect public perception of  
645 climate change and geohazards? An Italian case study. *Global and Planetary Change*,  
646 90, 152-157.  
647

648 Pieri, A. B., von Hardenberg, J., Parodi, A., & Provenzale, A. (2015). Sensitivity of  
649 Precipitation Statistics to Resolution, Microphysics, and Convective Parameterization:

650 A Case Study with the High-Resolution WRF Climate Model over Europe. *Journal of*  
651 *Hydrometeorology*, 16(4), 1857-1872.

652

653 Pinto, J. G., Ulbrich, S., Parodi, A., Rudari, R., Boni, G., & Ulbrich, U. (2013).  
654 Identification and ranking of extraordinary rainfall events over Northwest Italy: The  
655 role of Atlantic moisture. *Journal of Geophysical Research: Atmospheres*, 118(5),  
656 2085-2097.

657

658 Reale, O., Feudale, L., & Turato, B. (2001). Evaporative moisture sources during a  
659 sequence of floods in the Mediterranean region. *Geophysical research letters*, 28(10),  
660 2085-2088.

661

662 Rebora, N., Molini, L., Casella, E., Comellas, A., Fiori, E., Pignone, F., Siccardi, F.,  
663 Silvestro, F., Tanelli, S., & Parodi, A. (2013). Extreme rainfall in the mediterranean:  
664 what can we learn from observations?. *Journal of Hydrometeorology*, 14(3), 906-922.

665

666 Rodrigo, F. S. (2010). Changes in the probability of extreme daily precipitation  
667 observed from 1951 to 2002 in the Iberian Peninsula. *International Journal of*  
668 *Climatology*, 30(10), 1512-1525.

669

670 Schumacher, R. S., & Johnson, R. H. (2005). Organization and environmental  
671 properties of extreme-rain-producing mesoscale convective systems. *Monthly weather*  
672 *review*, 133(4), 961-976.

673

674 Silvestro, F., Rebora, N., Giannoni, F., Cavallo, A., & Ferraris, L. (2015). The flash  
675 flood of the Bisagno Creek on 9th October 2014: An "unfortunate" combination of  
676 spatial and temporal scales. *Journal of Hydrology*.

677

678 Silvestro, F., Rebora, N., Rossi, L., Dolia, D., Gabellani, S., Pignone, F., Trasforini, E.,  
679 Rudari, R., De Angeli, S., & Masciulli, C. (2016). What if the 25 October 2011 event  
680 that struck Cinque Terre (Liguria) had happened in Genoa, Italy? Flooding scenarios,  
681 hazard mapping and damage estimation. *Natural Hazards and Earth System Sciences*,  
682 16(8), 1737-1753.

683

684 Skamarock, W. C., Klemp, J. B., Dudhia, J., Gill, D. O., Barker, D. M., Duda, M.G.,  
685 Xiang-Yu, Wang, W., & Powers, J. G. (2008). A Description of the Advanced Research  
686 WRF Version 3 (No. NCAR/TN-475+STR). National Center for Atmospheric Research  
687 Boulder, Mesoscale and Microscale Meteorology Division.

688

689 Squitieri, B. J., & Gallus Jr, W. A. (2016). WRF Forecasts of Great Plains Nocturnal  
690 Low-Level Jet-Driven MCSs. Part II: Differences between Strongly and Weakly Forced  
691 Low-Level Jet Environments. *Weather and Forecasting*, 31(5), 1491-1510.

692

693 Stucki, P., Brönnimann, S., Martius, O., Welker, C., Rickli, R., Dierer, S., Bresch, D.N,  
694 Compo, G.P. & Sardeshmukh, P. D. (2015). Dynamical downscaling and loss modeling  
695 for the reconstruction of historical weather extremes and their impacts: a severe  
696 Foehn storm in 1925. *Bulletin of the American Meteorological Society*, 96(8), 1233-  
697 1241.

698

699 Thompson, G., Field, P. R., Rasmussen, R. M., & Hall, W. D. (2008). Explicit forecasts  
700 of winter precipitation using an improved bulk microphysics scheme. Part II:  
701 Implementation of a new snow parameterization. *Monthly Weather Review*, 136(12),  
702 5095-5115.

703  
704 Toreti, A., Xoplaki, E., Maraun, D., Kuglitsch, F. G., Wanner, H., & Luterbacher, J.  
705 (2010). Characterisation of extreme winter precipitation in Mediterranean coastal sites  
706 and associated anomalous atmospheric circulation patterns. *Nat. Hazards Earth Syst.*  
707 *Sci*, 10(5), 1037-1050.  
708  
709 Toreti, A., Giannakaki, P., & Martius, O. (2015). Precipitation extremes in the  
710 Mediterranean region and associated upper-level synoptic-scale flow structures.  
711 *Climate Dynamics*, 1-17.  
712  
713 Trenberth, K. E. (2011). Changes in precipitation with climate change. *Climate*  
714 *Research*, 47(1), 123.  
715  
716 Trouet, V., & Van Oldenborgh, G. J. (2013). KNMI Climate Explorer: a web-based  
717 research tool for high-resolution paleoclimatology. *Tree-Ring Research*, 69(1), 3-13.  
718  
719 Ward, P. J., Jongman, B., Weiland, F. S., Bouwman, A., van Beek, R., Bierkens, M. F.  
720 P., Ligtoet, W., & Winsemius, H. C. (2013). Assessing flood risk at the global scale:  
721 model setup, results, and sensitivity. *Environmental research letters*, 8(4), 044019.  
722  
723 Whitaker, J. S., Compo, G. P., Wei, X., & Hamill, T. M. (2004). Reanalysis without  
724 radiosondes using ensemble data assimilation. *Monthly Weather Review*, 132(5),  
725 1190-1200.  
726  
727 Ulbrich, U., Lionello, P., Belušić, D., Jacobeit, J., Knippertz, P., Kuglitsch, F. G.,  
728 Leckebusch, G.C., Luterbacher, J., Maugeri, M., Maheras, P., Nissen, K.M., Pavan, V.,  
729 Pinto, J.G., Saaroni, H., Seubert, S., Toreti, A., Xoplaki, E., & Ziv, B. (2012). Climate  
730 of the Mediterranean: synoptic patterns, temperature, precipitation, winds, and their  
731 extremes. In *The Climate of the Mediterranean Region-From the Past to the Future*.  
732 Elsevier, London.  
733  
734 Van den Besselaar, E. J. M., Klein Tank, A. M. G., & Buishand, T. A. (2013). Trends in  
735 European precipitation extremes over 1951–2010. *International Journal of*  
736 *Climatology*, 33(12), 2682-2689.  
737  
738 Violante, C., Braca, G., Esposito, E., & Tranfaglia, G. (2016). The 9 September 2010  
739 torrential rain and flash flood in the Dragone catchment, Atrani, Amalfi Coast  
740 (southern Italy). *Natural Hazards and Earth System Sciences*, 16(2), 333-348  
741  
742 Yair, Y., Lynn, B., Price, C., Kotroni, V., Lagouvardos, K., Morin, E., Mugnai, A., &  
743 Llasat, M.d.C. (2010). Predicting the potential for lightning activity in Mediterranean  
744 storms based on the Weather Research and Forecasting (WRF) model dynamic and  
745 microphysical fields. *Journal of Geophysical Research: Atmospheres*, 115, D04205.  
746  
747

748 **Tables and table captions**

749

<b>Parameter</b>	<b>Average</b>	<b>Standard deviation</b>
PAIRED CENTROID DISTANCE (km)	114	62
FCST AREA/OBS AREA	1.10	0.90
FCST INT 50/OBS INT 50	0.73	0.06
FCST INT 90/OBS INT 90	0.62	0.11
TOTAL INTEREST	0.88	0.09

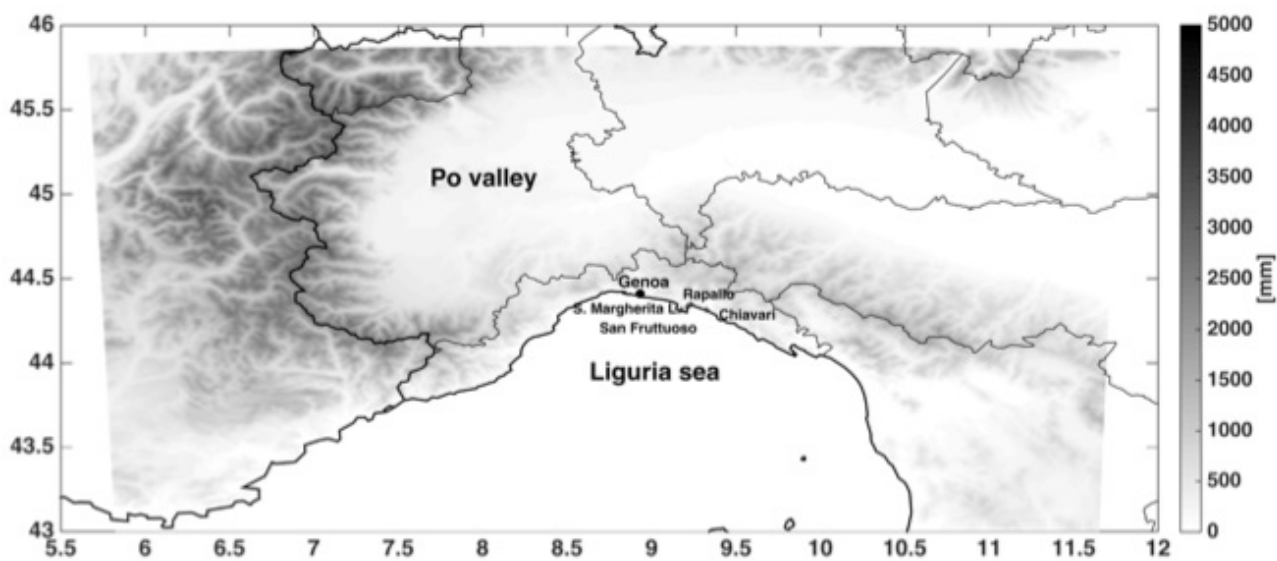
750

751 ***Table 1: Clusters pairs statistics for the 12 members out of 17, showing***  
752 ***significant values (above 0.8) of the total interest function.***

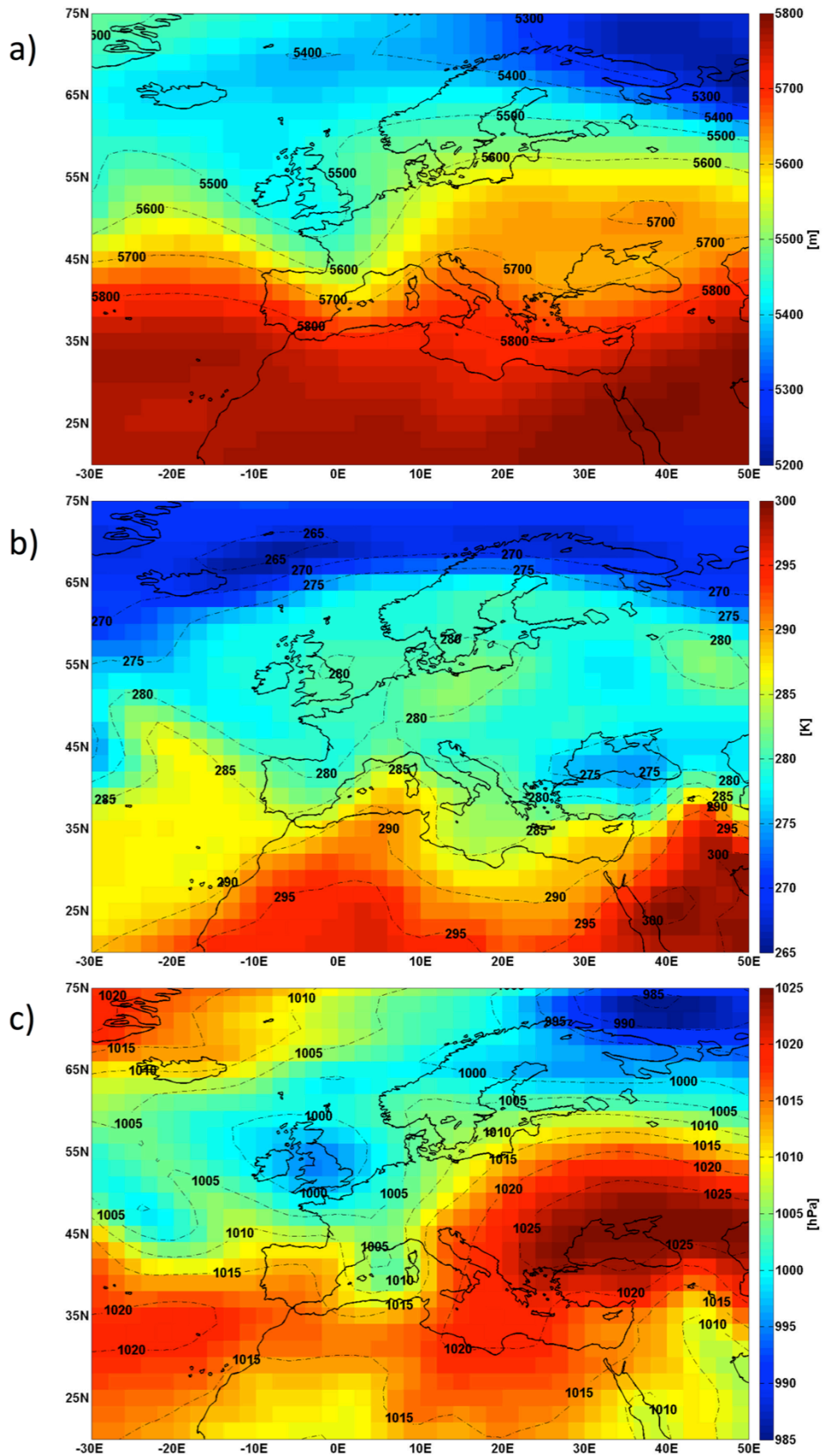
753

754

755 **Figures and figure captions**  
756



757  
758 Figure 1: Study region and Liguria coastal cities affected by the September 1915  
759 event.



760

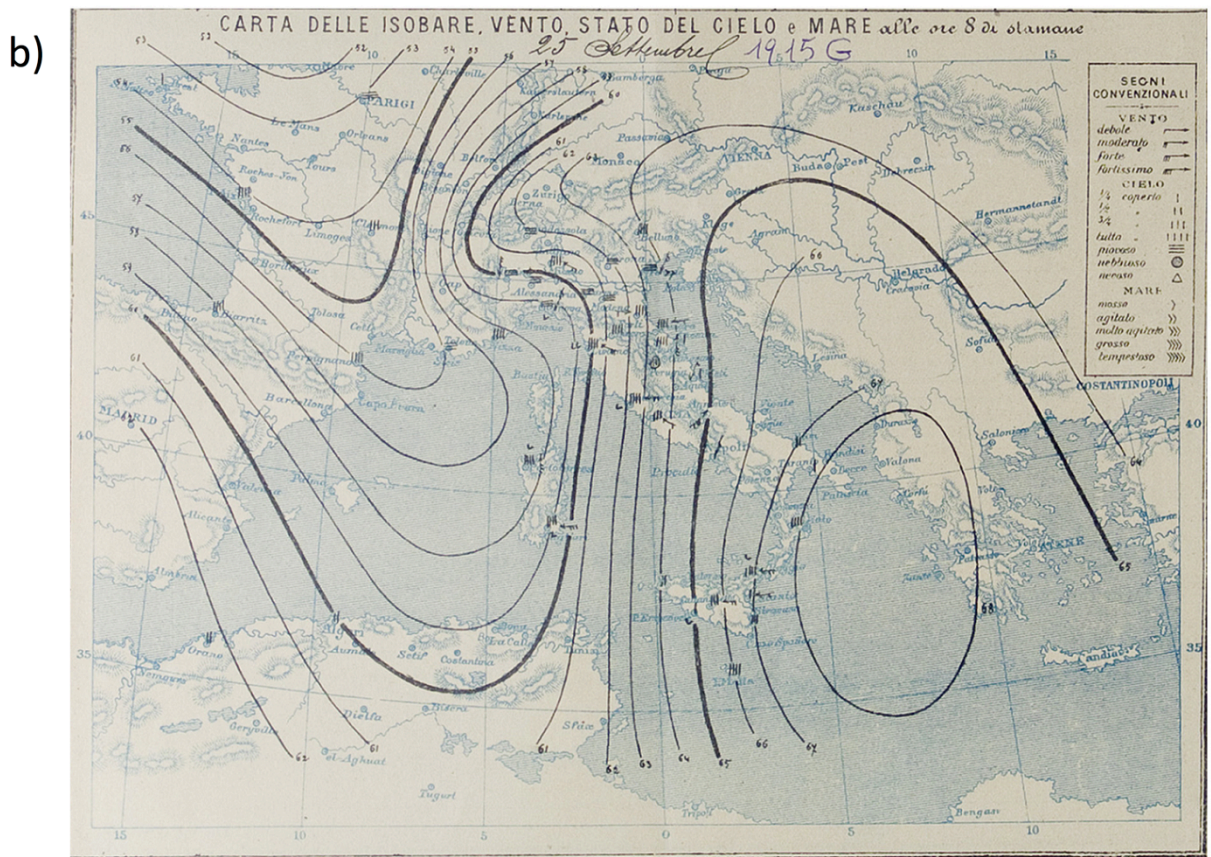
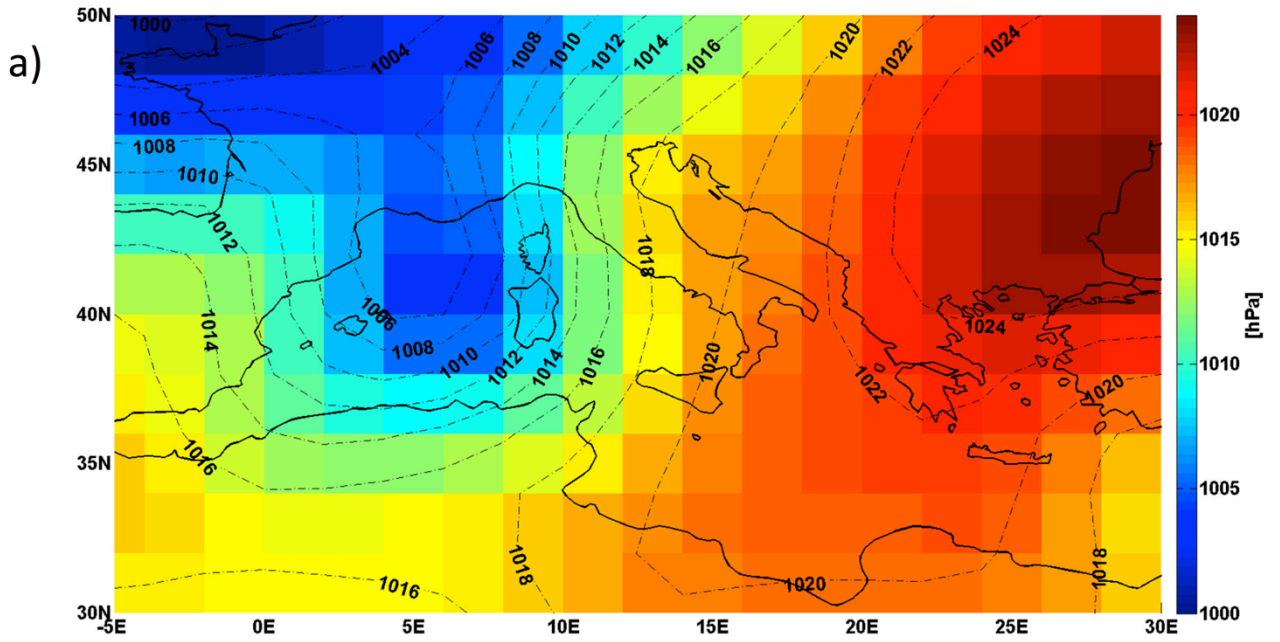
761

762

763

Figure 2: a) 500 hPa geopotential, b) 850 hPa temperature, and c) sea level pressure on 25<sup>th</sup> September, 1915 06UTC (20<sup>th</sup> Century Reanalysis Project mean fields over the 56 ensemble members).





764

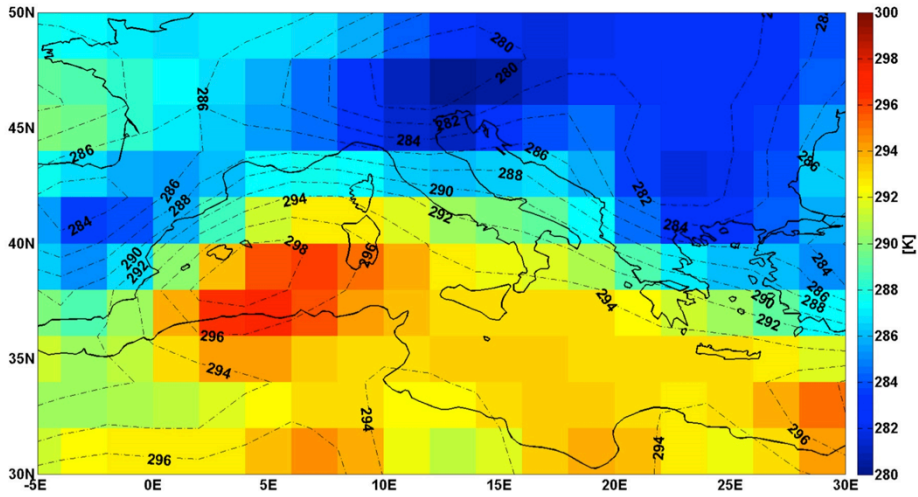
765

766

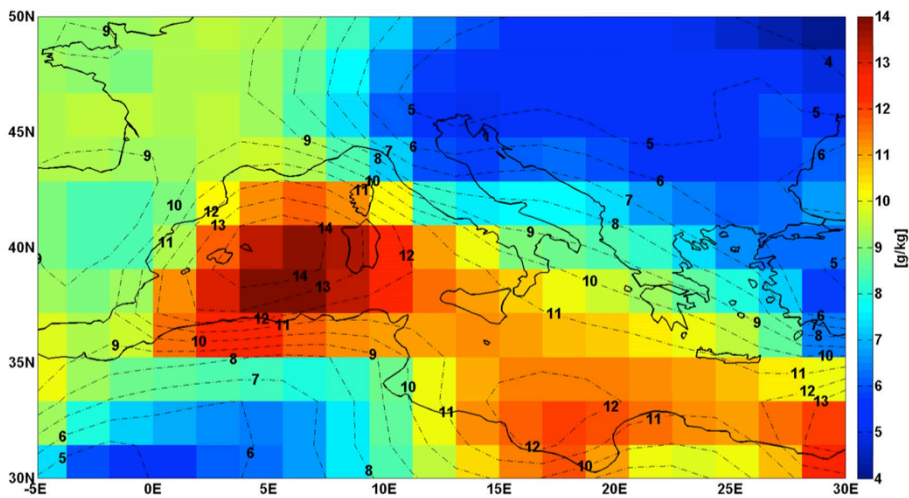
767

Figure 3: a) sea level pressure isobars on 25<sup>th</sup> September 1915 at 07UTC, as provided by the Italian Royal Meteorological Service. b) the same field as in figure 2c, but over the same area of the map in figure 3a.

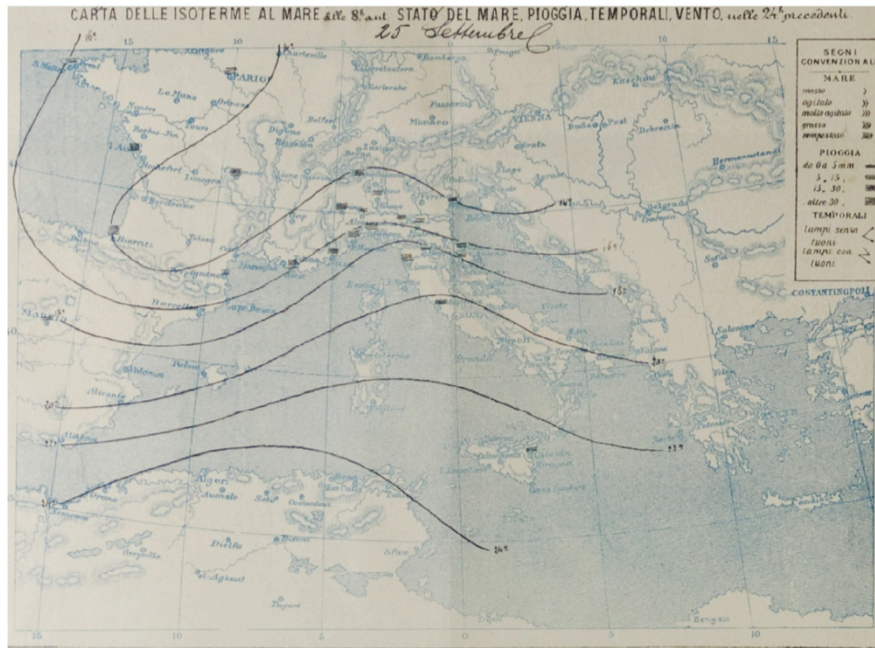
a)



b)



c)

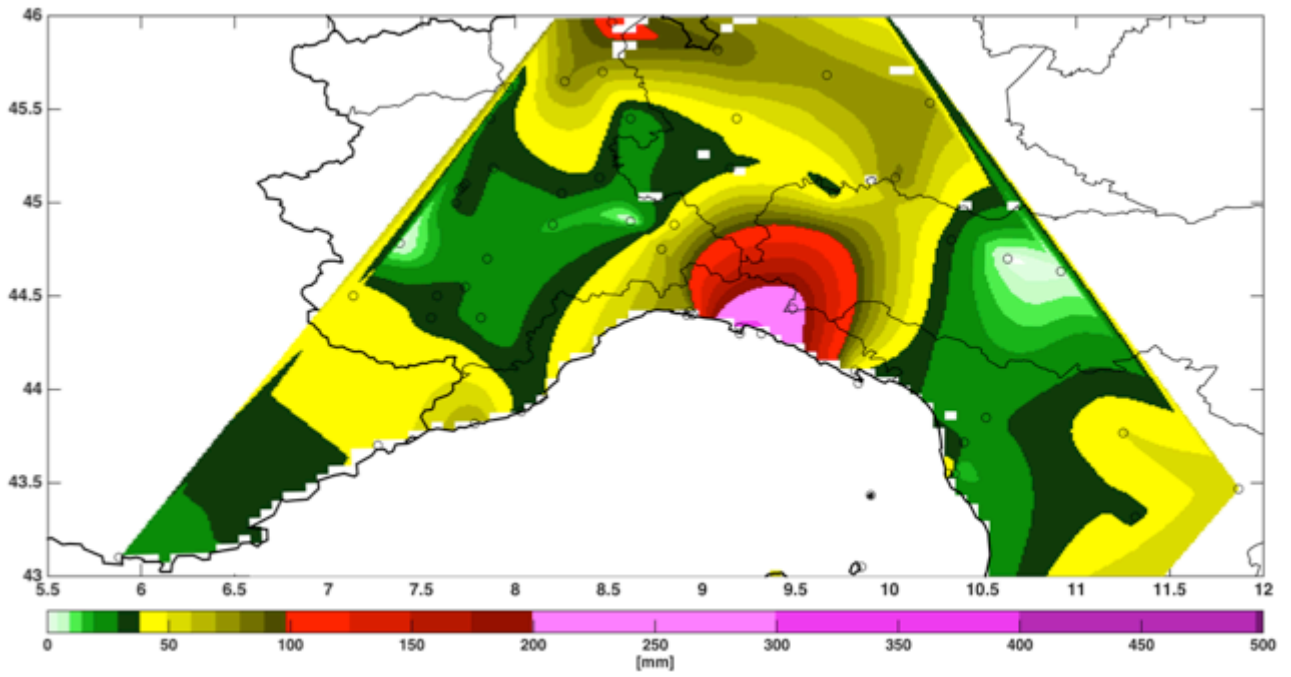


768

769 Figure 4: a) 2 m temperature and b) 2 m specific humidity on 25<sup>th</sup> September 1915  
 770 (06 UTC) over the study region. (20th Century Reanalysis mean fields over the 56  
 771 ensemble members), c) surface temperature isotherms on 25<sup>th</sup> September 1915  
 772 (07UTC), as provided by the Italian Royal Meteorological Service.



773



774

775 Figure 5: Quantitative precipitation estimates (QPE) for 24<sup>th</sup> September 07UTC - 26<sup>th</sup>  
776 September 1915 07UTC.

777

778

779

780

781

782

783



784



785

786

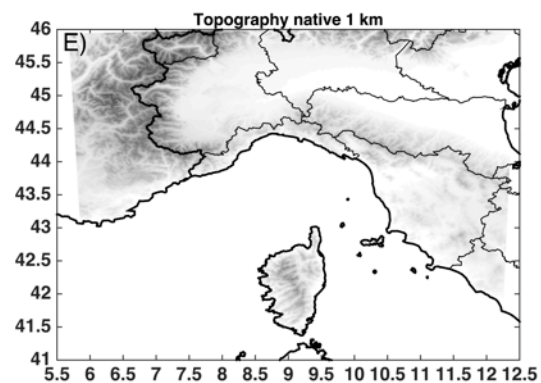
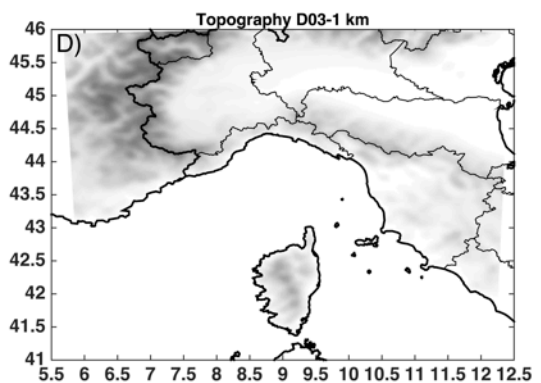
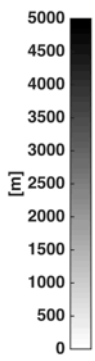
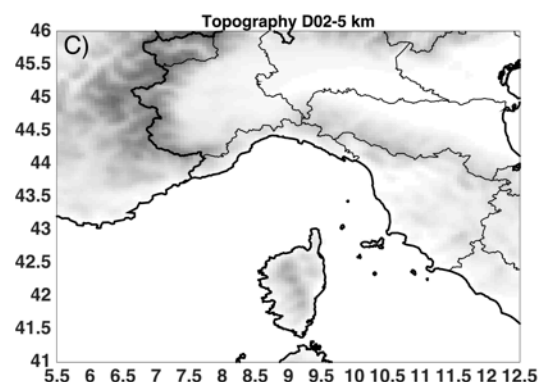
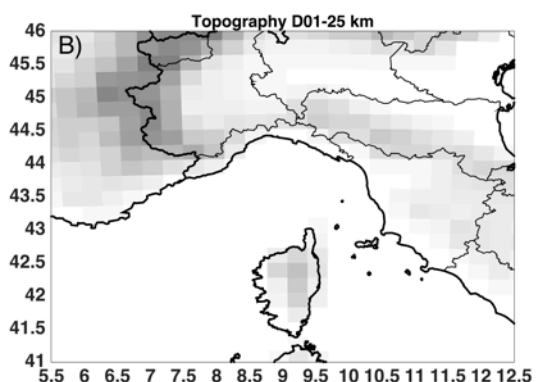
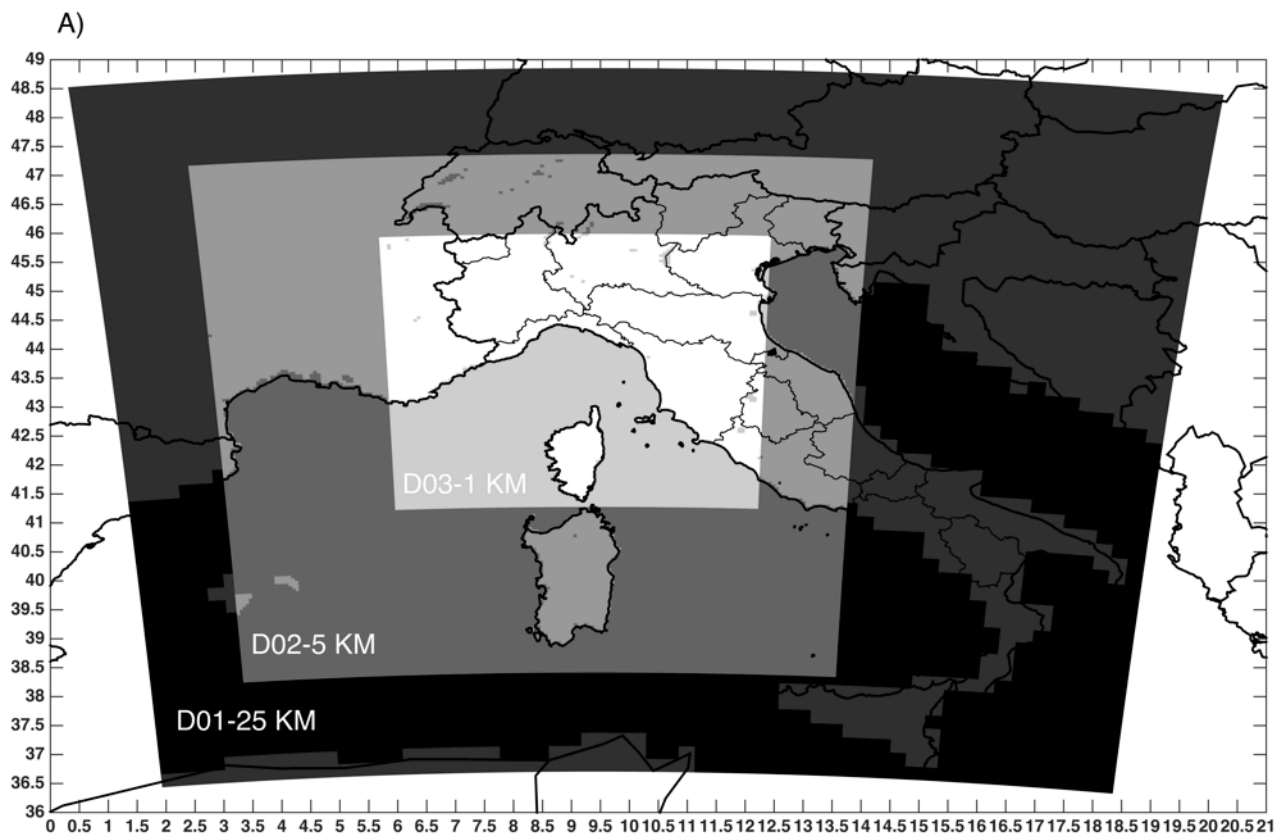
787 Figure 6: Rapallo flash-flood impacts on 25<sup>th</sup> September 1915 (Courtesy of real estate  
788 Agency Bozzo in Camogli).

789

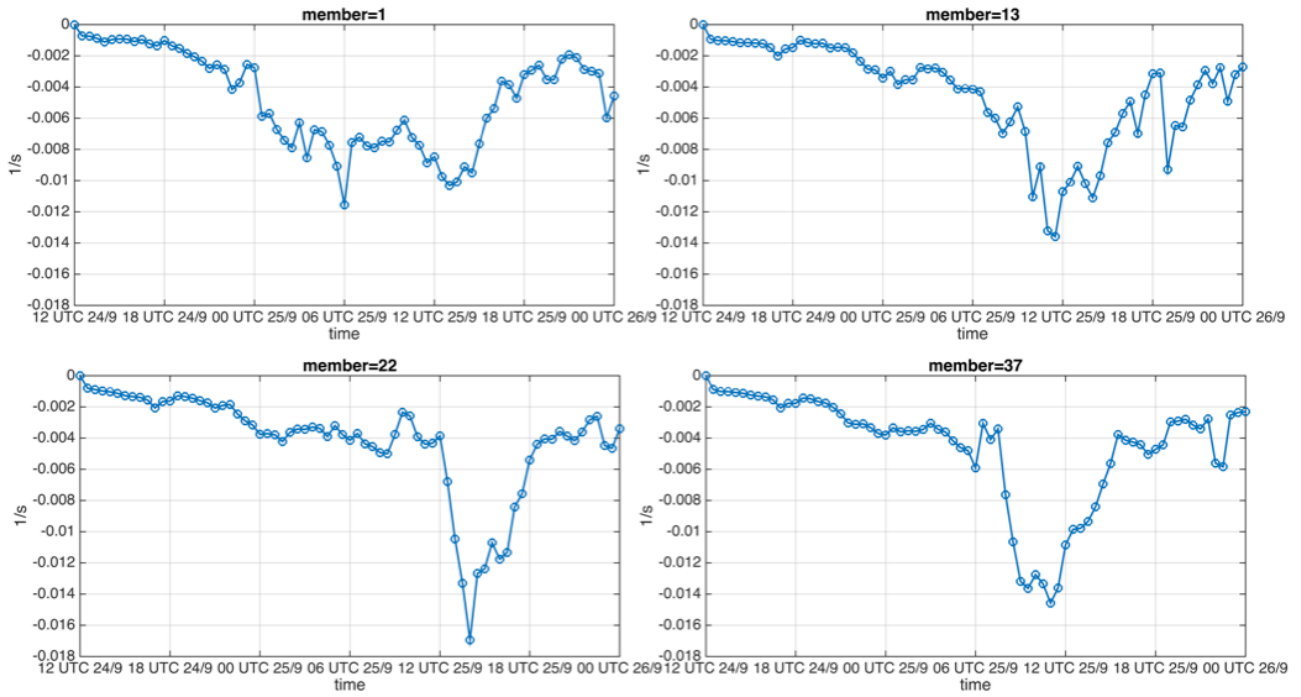
790

791





795  
 796 Figure 8: Panel a: domains for the numerical simulations of the Genoa 1915 event,  
 797 d01 ( $\Delta=25$  km), d02 ( $\Delta=5$  km) and d03 ( $\Delta=1$  km). Panels b-e compare the  
 798 topography over the d03 area, for d01, d02, d03, and native 1 km grid spacing.



799

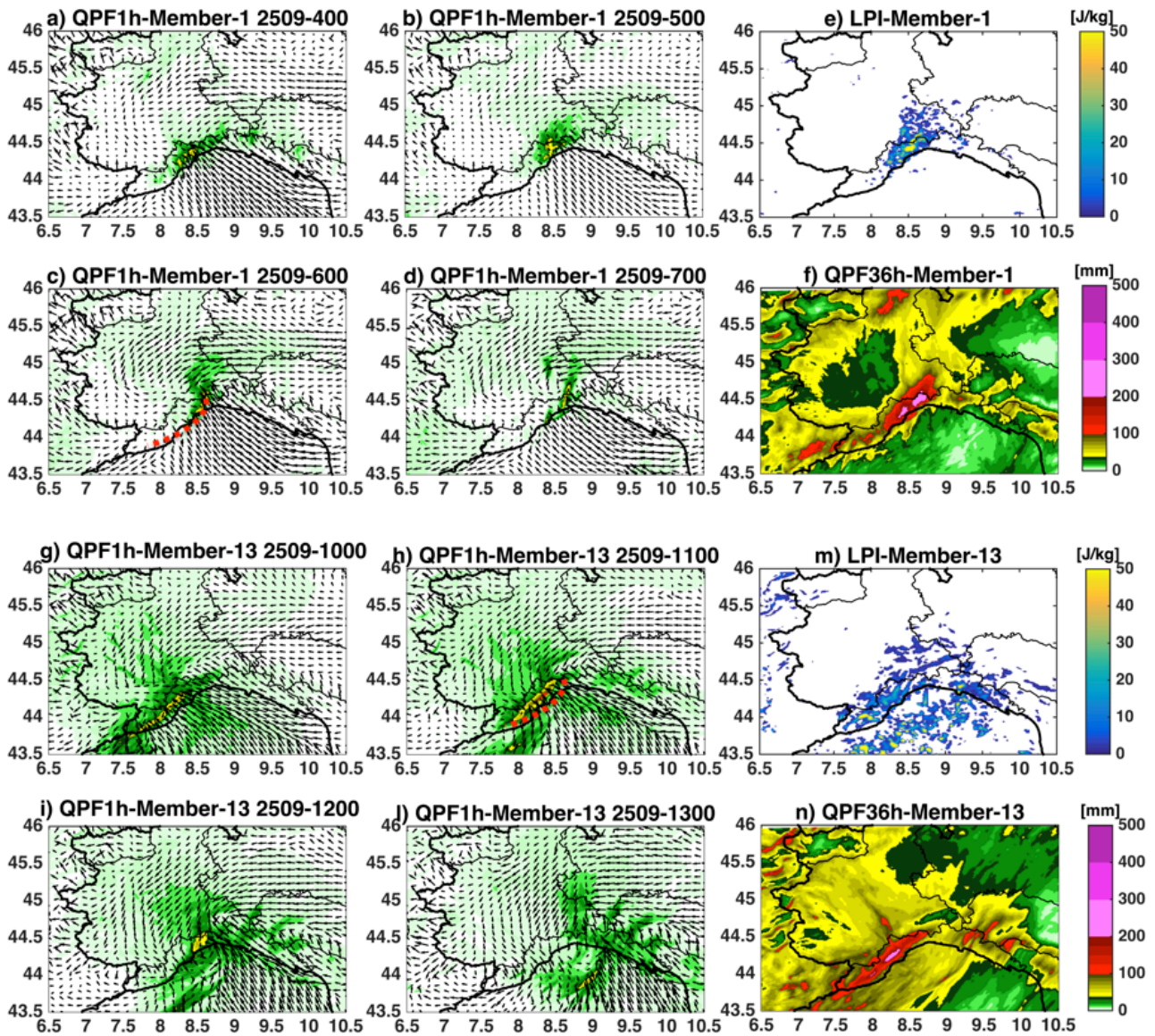
800

801

802

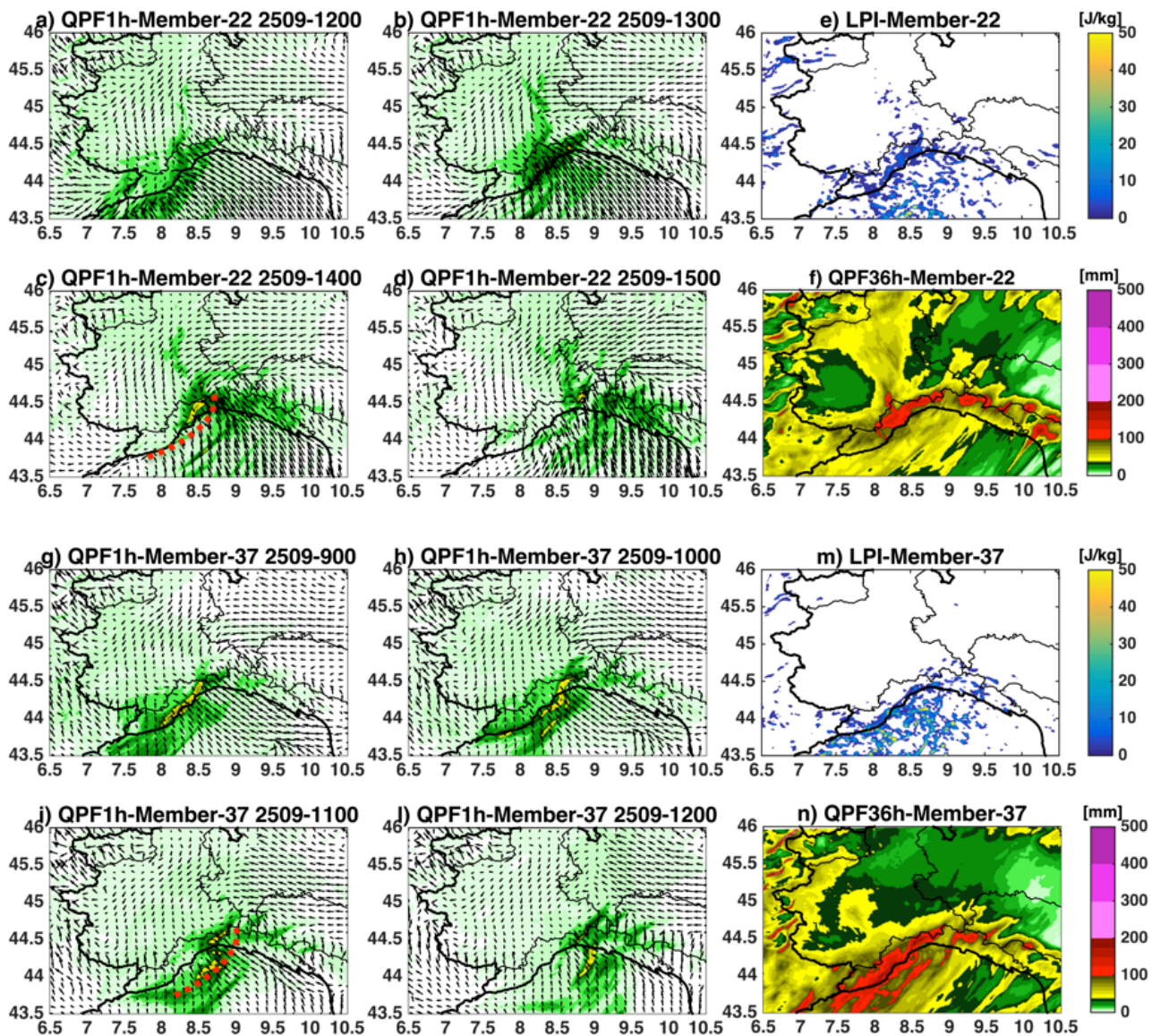
Figure 9: Minimum divergence time series (1/s) for members 1, 13, 22 and 37.





803

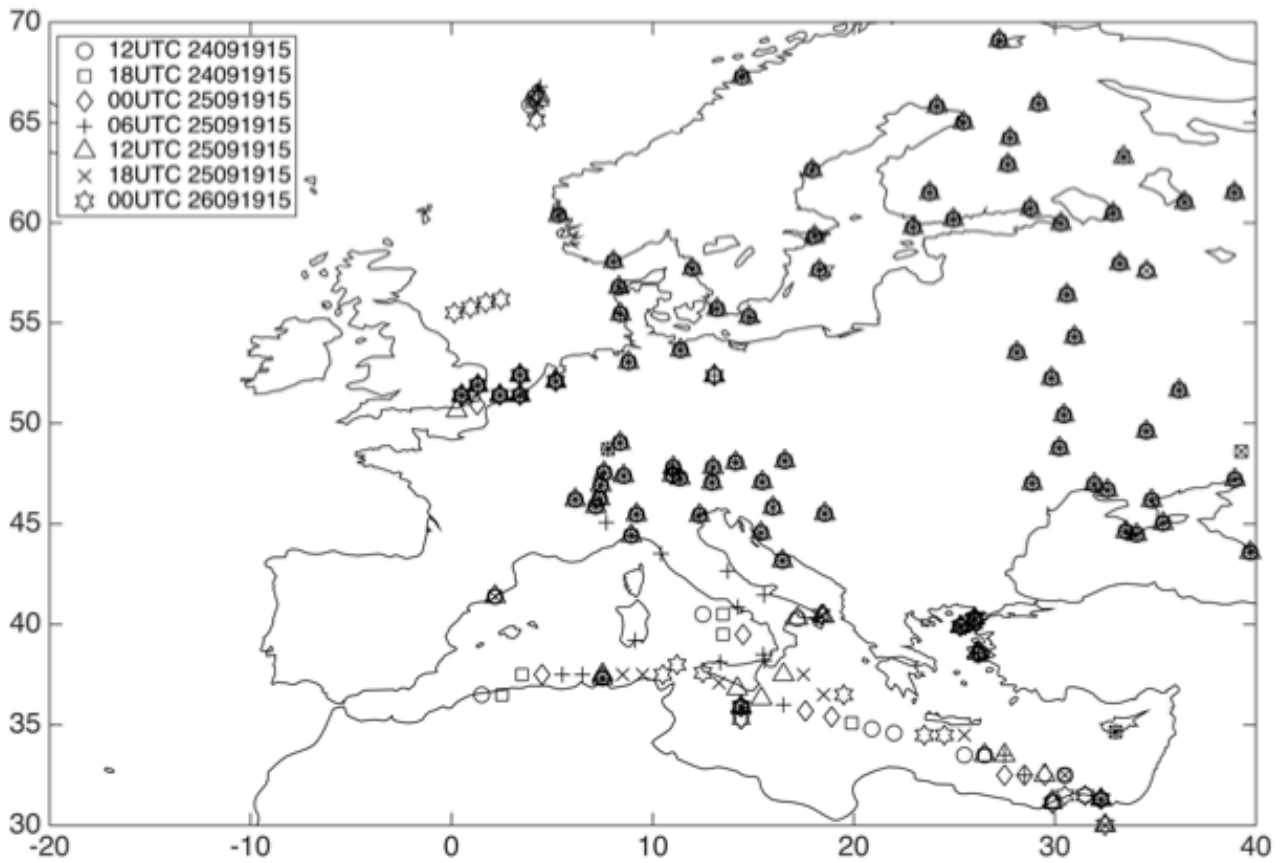
804 Figure 10: Panels a-d, and g-l show the hourly QPF and 10 m wind fields  
 805 corresponding to the period with the minimum divergence values in Figure 9 for  
 806 members 1, and 13 (the convergence line trace in the most active phase is red  
 807 dashed). Panels e-f, and m-n show the Lightning Potential Index accumulated over  
 808 the same 4 hours period, and the 36 hour QPF, respectively for members 1, and 13.



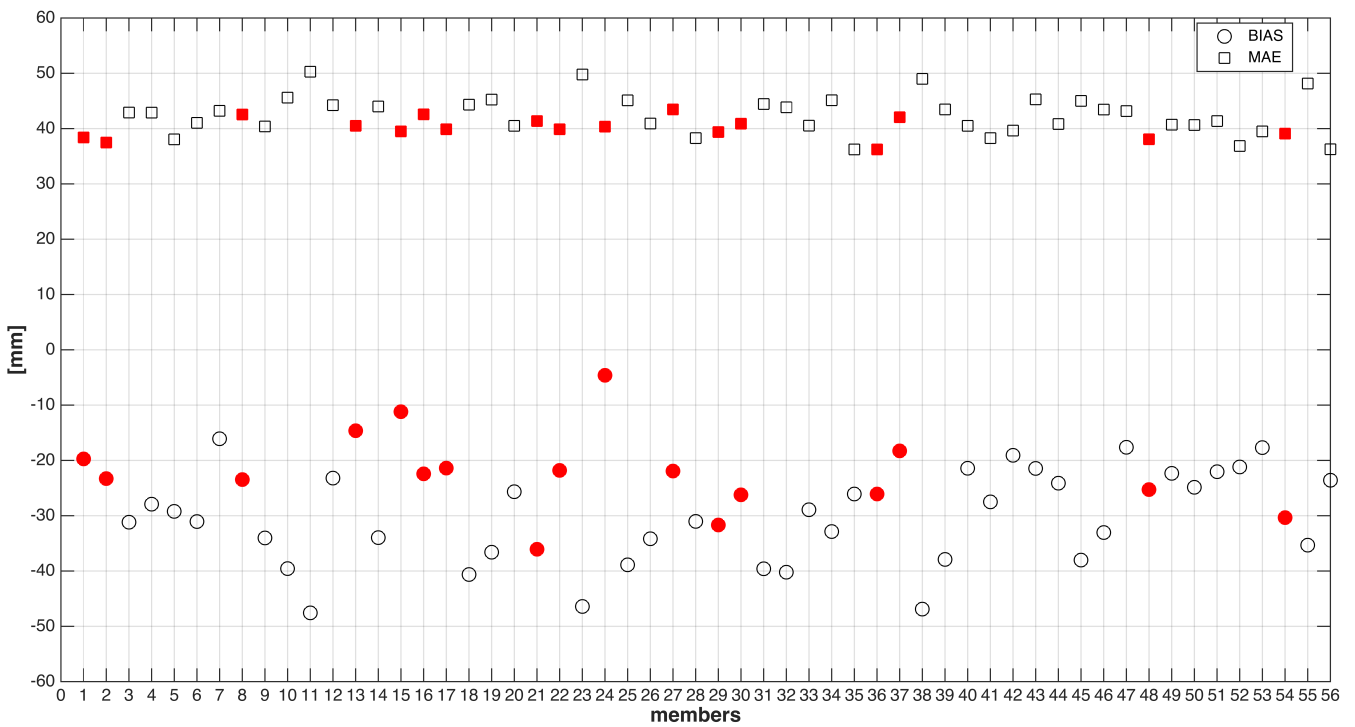
809

810 Figure 11: Panels a-d, and g-l show the hourly QPF and 10 m wind fields  
 811 corresponding to the period with the minimum divergence values in Figure 9 for  
 812 members 22, and 37 (the convergence line trace in the most active phase is red  
 813 dashed). Panels e-f, and m-n show the Lightning Potential Index accumulated over  
 814 the same 4 hours period, and the 36 hour QPF, respectively for members 22, and 37.





815  
 816 Figure 12: Surface pressure stations assimilated every six hours in the period 12UTC  
 817 24<sup>th</sup> September 1915 - 00UTC 26<sup>th</sup> September 1915.

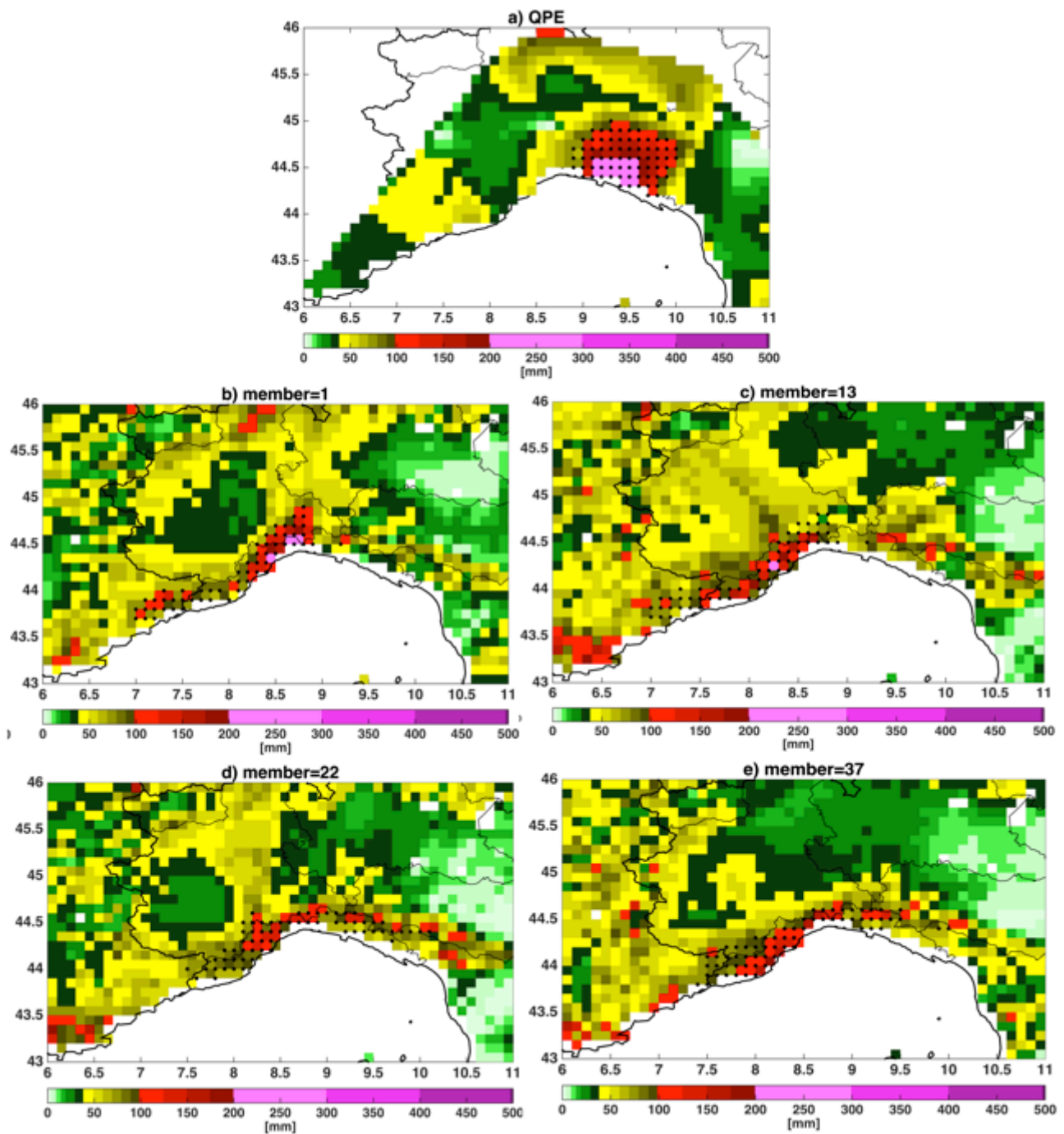


818  
 819 Figure 13: Rainfall depth BIAS and MAE for each d03-1km WRF member. Red markers  
 820 represent the 17 members producing robust and persisting convergence lines over the  
 821 Liguria Sea.



822

823



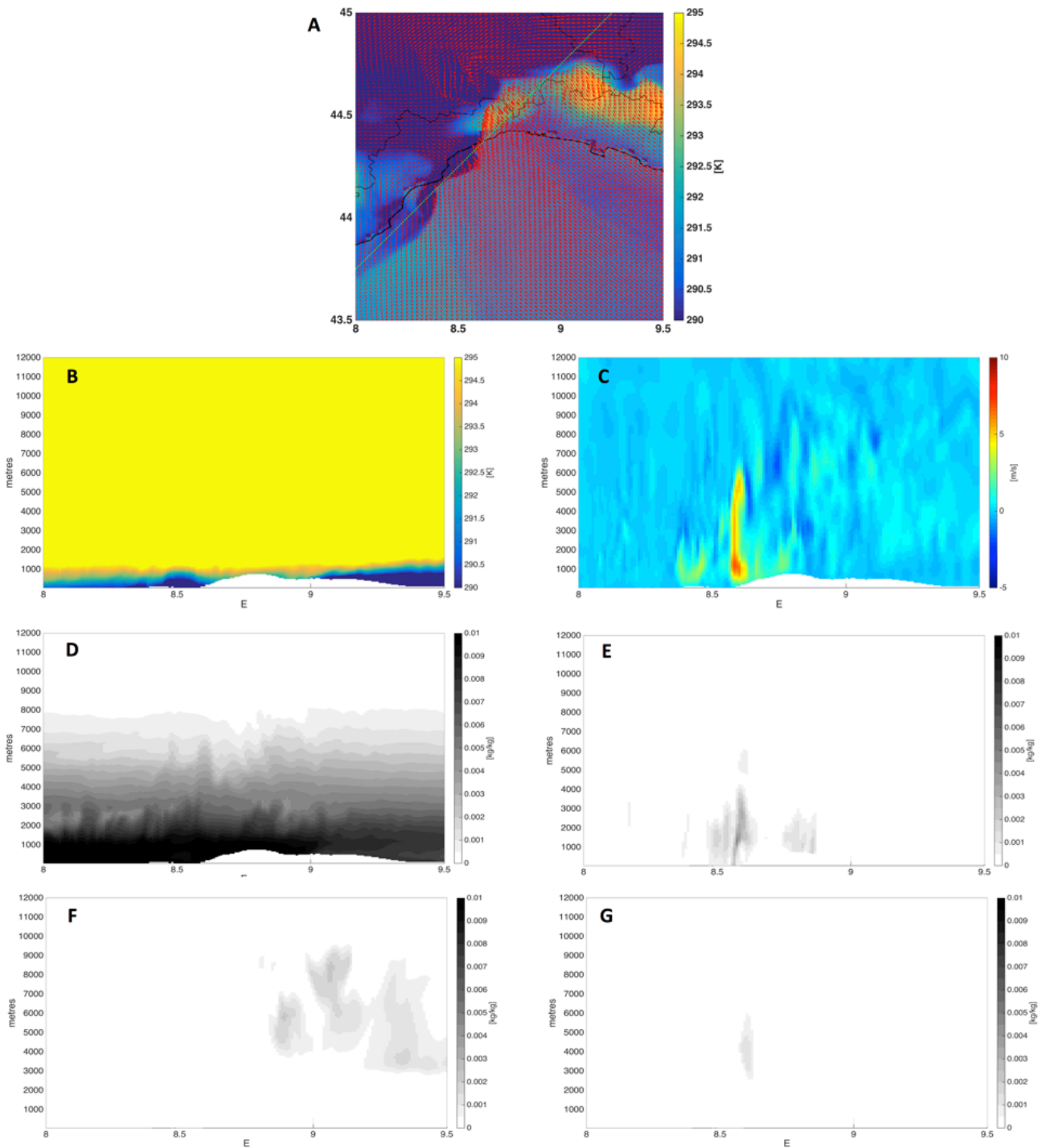
824

825

826

827

Figure 14: QPE regridded at 10 km grid spacing (panel a) and QPF from members 1 (panel b), 13 (panel c), 22 (panel d) and 37 (panel e), regridded at 10 km grid spacing (lower panels). Dots identify the areas of paired clusters.



828  
 829 Figure 15: Member 1, 06UTC on 25 september 1915. Panel A shows the 2 m potential  
 830 temperature field together with the 10 m horizontal wind vector field. Panel b to g  
 831 shows, instead, the vertical cross sections of potential temperature, vertical velocity,  
 832 water vapour, rain water, snow, and graupel mixing ratios along the cross section  
 833 (green dotted) shown in panel a.

834